 doi:10.20944/preprints201907.0129.v1

On the Investigation of Temperature Effects on Oil Relative Permeability: Robust Modeling and Data Assessments

Shahaboddin Shamshirband 1,2[*], Alireza Baghban[3], Jafar Sasanipour[4], Masoud Hadipoor[5],

[1]Department for Management of Science and Technology Development, Ton Duc Thang University, Ho Chi Minh City, Viet Nam

[2]Faculty of Information Technology, Ton Duc Thang University, Ho Chi Minh City, Viet Nam

[3] Chemical engineering Department, Amirkabir University of Technology, Mahshahr Campus, Mahshahr, Iran.

[4]Department of Gas Engineering, Ahwaz Faculty of Petroleum Engineering, Petroleum University of Technology (PUT), P.O. Box 63431, Ahwaz, Iran.

[5]Petroleum engineering Department, Petroleum University of Technology, Ahwaz, Iran.

Abstract

Various empirical models are available to evaluate the temperature effects on relative permeability of the different rock and fluid systems. However, the implementation of limited experimental data points may hinder the applicability of such models to other systems. This study aims to develop new predictive models for k_{ro} estimation based on multilayer perceptron artificial neural network (MLP-ANN), adaptive neuro-fuzzy inference system (ANFIS), and least squares support vector machine (LSSVM) approaches. A database comprising of 626 data points applied to the model development. The independent variables are temperature, oil viscosity, water viscosity, water

[*] Corresponding author
S.Shamshirband (shahaboddin.shamshirband@tdtu.edu.vn)

 doi:10.20944/preprints201907.0129.v1

saturation (S_w), and the absolute permeability. Each variable covers a wide range of variations which increases models' potential to be applied in various systems with different characteristics. The doubtful experimental data points excluded using a leverage value approach and a sensitivity analysis carried out to determine the quantitative impact of every individual independent variable on the k_{ro}. Statistical error analyses demonstrated the coefficient of determination (R^2) values of 0.985, 0.975, and 0.999 for MLP-ANN, ANFIS, and LSSVM, respectively. The comparative study indicated that the LSSVM had the best performance regarding both graphical and statistical error analyses among the newly proposed models and previously reported models in the literature.

Keywords: Relative permeability; Multilayer perceptron artificial neural network; ANFIS; LSSVM; Heavy oil.

1. Introduction

There is a huge variety of thermal enhanced oil recovery (EOR) techniques. Two of the most applied methods are cyclic steam stimulation (CSS) and steam assisted gravity drainage (SAGD) [1,2]. Thermal EOR methods work based on creating high-temperature conditions, which significantly reduces viscosity and enables effective mobilization of highly viscous oils such as bitumen. In addition to viscosity reductions due to thermal EOR techniques, using these technics lead to a reduction in densities, interfacial tensions (IFTs), and changes the composition of oil, wettability and so forth [3,4]. The amount of k_{ro} and k_{rw} in a reservoir is also affected by such variations. Therefore, permeability variations have to be considered in developing a reliable thermal processing model. Many studies have been investigating temperature effects on permeability variation of different porous systems with different oils. Edmonson [5] performed an unsteady state measurement. He conducted a study using heavy crude oil and light refined oil, Berea sandstone cores, and temperature ranging from 24-260°C. Results indicated that higher S_w

Preprints (www.preprints.org) | NOT PEER-REVIEWED | Posted: 9 July 2019 doi:10.20944/preprints201907.0129.v1

result in lower oil/water ($\frac{K_{ro}}{K_{rw}}$), while lower S_ws are associated with higher $\frac{K_{ro}}{K_{rw}}$. Residual oil saturation (S_{ro}) also had a decreasing trend as temperature increased. Edmonson proposed that IFT variation and viscosity ration modification are reasons for such an observation. Similar results are reported by Davidson [6] for a system of white oil, stilled water, clean sandpack, and temperature ranging from 22 to 282°C. Irreducible water saturation (S_{rw}) effect on k_{ro} and k_{rw} of the oil/water system at high-temperature conditions is also investigated by Davidson [6]. Poston et al. [7] studied the wettability alteration and stated that both high temperature and viscosity ratio modification would alter wettability. They reported increasing S_{rw}, oil/water permeability variation, and oil saturation reduction at high-temperature conditions [7]. Unlike Poston et al. who stated increasing tendency towards strong water-wetness at elevated temperature, Miani and Okazawa [8] and Miani and Batycky [9] believed that heavy oil endpoint permeability reduction and water permeability increment at high temperatures is due to more tendency towards weak wetness. In contrast to the aforementioned statements by Poston et al. [7], Miani and Okazawa [8], and Miani and Batycky [9], Esfahani et al. [10] observed decreasing and increasing trends for water and S_{ro} at elevated temperatures, respectively. They reported viscosity ratio effects on k_{ro} and k_{rw} at high-temperature conditions. They conducted their study using limestone and dolomite core plug samples and investigated rock's wettability by Amott [11] and USBM [12] tests. Based on the Amott-Harvey index, they stated that temperature increment results in an increasing tendency towards oil-wetness. Polikar et al. [13,14] stated that k_{ro} and k_{rw} are insensitive to temperature. However, they reported a variation of endpoint k_{ro} and k_{rw}, S_{ro}, and S_{rw} at 250°C. They related these variations to water phase solubility in large oil volume at high temperature, heterogeneities of porous media, and unstable displacement.

Preprints (www.preprints.org) | NOT PEER-REVIEWED | Posted: 9 July 2019 doi:10.20944/preprints201907.0129.v1

Although Ashrafi et al. [15,16] observed increasing S_w at high temperatures, they stated that no apparent trend is found to clearly linking k_{ro} and temperature. A tendency towards water-wetness and consequently higher S_{rw} are reported by Weinbrandt et al. [17] for a system with white oil #15 and Boise sandstone.

Bennion et al. [18] investigated the brine endpoint k_{rw} at elevated temperatures. They reported brine endpoint k_{rw} reduction due to pore damage and wettability alteration phenomena. As you can see there are various contradictory statements about temperature effects on k_{ro} and k_{rw} [19–30].

Indirect investigation of temperature effects has been conducted by some authors. For instance, contact angle variation was considered by Ehrlich [31] in an analytical investigation of temperature effects on two-phase k_{ro} and k_{rw}. Amaefule et al. [32] proposed an IFT based relative permeability model to investigating temperature effects. According to this model, S_{rw} and S_{ro} decline if the capillary number exceeds a specific value. Results of an study by Torabzadey et al. [33] was implemented by Kumar et al. [22] to develop an representing correlation for k_{ro} and k_{rw}. They classified experimental results as high IFT and low IFT systems. They considered the temperature effects by implementing an adjustable coefficient that could change under different temperature conditions, rock and fluid properties.

Artificial neural networks (ANNs) are widely applied in different scientific fields. They are suitable approaches to be applied when the establishment of certain data trends is required [34,35]. However, more efforts have to be made regarding the appropriate implementation of ANNs in EOR application. The ANFIS method also have found many applications since they benefit advantages of both ANNs and fuzzy logic systems [34,36]. Support vector machine (SVM) strategy is proposed by Vapnik [37] in the 1990s in order to overcome artificial neural network's deficiencies such as overfitting, local minima prediction, and inconsistency [38]. The SVM

Preprints (www.preprints.org) | NOT PEER-REVIEWED | Posted: 9 July 2019 doi:10.20944/preprints201907.0129.v1

strategy is developed based on statistical learning theory and has found various applications [39–43]. The LSSVM method, a modified version of SVM, is proposed to reduce the SVM's complexity. LSSVM is applied in different applications such as estimating solid component solubility in supercritical CO2 [44], dew point pressure estimation in gas condensate systems [45], natural gas viscosity prediction [46], and crude oil's saturation pressure prediction [47]. A data-driven model based on LSSVM approach was developed by Esmaeili et al. in order to estimate k_{ro} and k_{rw} by considering temperature variations [48]. It was an accurate model with R-squared value of 0.99. Beside the LSSVM approach which was developed in Esmaeili et al. work, we effort in this study to develop precise models based on three categories of artificial intelligence approaches and compare the results with other previously published models.

In the present work, the MLP-ANN, ANFIS, and LSSVM strategies are utilized to develop accurate and reliable predictive oil relative permeability (k_{ro}) models. In addition, as a novelty of work, application of three different strategies of artificial intelligence in this field was comprehensively compared with each other. Five independent variables, i.e. temperature (T), oil viscosity (μ_o), water viscosity (μ_w), water saturation (S_w), and absolute permeability of porous medium (k) are considered in process of model development.

2. Data Acquisition

2.1. Relative Permeability

Although several models for k_{ro} have been proposed, taking capillary pressure or S_w into consideration [49–55], few models consider the effects of temperature on k_{ro} and k_{rw} curves [18,56–58]. Bennion et al. [18] considered two separated temperature zones with a missing temperature zone, 100-150℃, where no information is given. Oil to water viscosity ratio was considered as the key parameter in Mosavat et al. work [57], conducted according to the data used

Preprints (www.preprints.org) | NOT PEER-REVIEWED | Posted: 9 July 2019 doi:10.20944/preprints201907.0129.v1

by Miani and Okazawa [8] and Wang et al. [59]. Torabi et al. [56] developed a model based on normalized pressure, μ_o, and water injection rate values. The inclusion of temperature as a specific parameter is carried out by Zhang et al. [58]. Where they applied empirical correlations for S_{ro} and S_{rw}, and endpoint K_{ro} and K_{rw} involved in relative permeability.

Data Selection

Various investigation focused on the effects of temperature on the k_{ro} and k_{rw}. However, few of them represented detailed information about experimental parameters. **Table 1** represents the database that we applied in this study to propose new k_{ro} and k_{rw} prediction models.

The amount of k_{ro} and k_{rw} is affected by changes in wettability, contact angle, and porous media type. Although the majority of researchers prefer conducting experiments using sand material, there are others who applied limestone, chalk, dolomite, Teflon, and Diatomite porous media [10,19,23,29,60–62]. The present study employs a database consisting of sand based porous media systems with light or heavy oil data points. Hence, the k_{ro} parameter is collected and summarized in **Table 1**. This table also reports the temperature, μ_o, permeability, and porosity ranges of the collected data points. 626 data points are collected from nine different studies, showing some permeability variations as a result of temperature alteration. As reported in this table, the oil viscosity ranges from 0.4192 to 1190 cP. Temperature and permeability also vary in the ranges of 152-95000mD, and 21.1-200℃, respectively. The present study aims to propose models based on MLP-ANN, ANFIS, and LSSVM approaches to link the temperature and permeability characteristics. The collected data points are separated into two main sets. One set is considered as the training and the other was used as testing. The training (75% of the total data point) and testing datasets are used to training the developed model and evaluating the models' performances over data points that are completely new to model.

Preprints (www.preprints.org) | NOT PEER-REVIEWED | Posted: 9 July 2019 doi:10.20944/preprints201907.0129.v1

3. Methodology

3.1. Multilayer Perceptron Artificial Neural Network (MLP-ANN)

Artificial neural networks (ANNs) are powerful modeling techniques that are capable of improving efficiency and learning from experiences [63]. ANNs are similar to our neural system, they have processing units, called neurons, which act as the biological cells in order to construct different layers of the artificial neural network. The network architecture is defined by the existing interconnection pattern between different neurons of the artificial neural network. The MLP-ANN offers an absolutely powerful problem-solving architecture [63]. In this architecture, each neuron connects to several neighbors with different weights which implies the relative influence of different neurons on other neurons. The three-layer structure of the MLP-ANN method is the typical form of this system which includes input and the output layers as the exterior layers and the hidden layers as the interior layers. Each layer consists of numerous neurons. The weighted summation of the input layer is transmitted to the interior layers and transformed by means of a specified activation function. Similarly, the output of the hidden layer undergoes a transformation in the output layer. The following formulation represents the MLP-ANN output:

$$\gamma_{jk} = F_k\left(\sum_{i=1}^{N_{k-1}} w_{ijk}\gamma_{i(k-1)} + \beta_{jk}\right) \quad (1)$$

where γ_{jk} and β_{jk} are the jth neuron of the kth layer output and bias weight, respectively. W_{ijk} and F_k also represent the link weights and transformation function, respectively. MLP-ANN architecture is schematically illustrated in **Figure 1**.

3.2. Adaptive Neuro-Fuzzy Inference System (ANFIS)

At the first place, the concept of fuzzy logic was proposed by Zade [64]. Unlike classical logic, fuzzy logic is capable of stating conclusions that lie between completely true and completely false

Preprints (www.preprints.org) | NOT PEER-REVIEWED | Posted: 9 July 2019 doi:10.20944/preprints201907.0129.v1

states [64]. ANFIS strategy enables benefitting advantages of both fuzzy logic systems and artificial neural networks, which results in precise solutions to complex and extremely non-linear problems [65,66]. There are two fuzzy inference system structures: (1) Mamdani, and (2) Takagi-Sugeno [67–69]. A Mamdani fuzzy inference system uses the logical definition to develop the *if-then* rules; but in the Takagi-Sugeno method, the *if-then* rules are based on available experimental data. The Takagi-Sugeno type fuzzy inference system is applied in ANFIS structure [68]. The following *if-then* rules are typically implemented in an ANFIS model development with two input parameters:

If X_1 and X_2 determined to be A_1 and B_1 then $f_1=m_1X_1+n_1X_2+r_1$ (2)

If X_1 and X_2 determined to be A_2 and B_2 then $f_2=m_2X_1+n_2X_2+r_2$ (3)

If X_1 and X_2 determined to be A_1 and B_2, respectively; then $f_3=m_3X_1+n_3X_2+r_3$ (4)

If X_1 and X_2 determined to be A_2 and B_1, respectively; then $f_4=m_4X_1+n_4X_2+r_4$ (5)

Where A_k and B_k for $k=1,2$ represent the fuzzy sets of X_1 and X_2, respectively and f represents the final result of the *if-then rule*.

Generally, the ANFIS configuration consists of five consecutive layers. **Figure 2** shows a schematic structure of an ANFIS system. The first layer is named the fuzzification layer and prepare input data for the next layers by utilizing specified membership functions. In this study, a Gaussian membership function was employed.

$$O_i^1 = \beta(X) = exp\left[-\frac{1}{2}\frac{(X-Z)}{\sigma^2}\right] \quad (6)$$

Preprints (www.preprints.org) | NOT PEER-REVIEWED | Posted: 9 July 2019 doi:10.20944/preprints201907.0129.v1

Where O is the output of the first layer, z denotes the Gaussian center, and σ^2 represents the variance. The Gaussian membership function parameters, z and σ^2, need to be optimized in order to determine the most accurate predictions.

The second layer determines the statements' reliability in antecedent parts through calculation of the so-called firing strength parameters:

$$O_i^2 = w_i = \beta_{Ai}(X)\beta_{Bi}(Y) \quad (7)$$

These firing strengths are then normalized in the third layer, using the following expression:

$$O_i^3 = \overline{w}_i = \frac{w_i}{\sum_i w_i} \quad (8)$$

Fourth layer uses the following expression:

$$O_i^4 = \overline{w}_i f_i = \overline{w}_i(m_i X_1 + n_i X_2 + r_i) \quad (9)$$

Where linear values of m_i, n_i, and r_i must undergo an optimization process.

Eventually, a summation procedure will be carried out to determine the final result in layer five:

$$O_i^5 = \sum_i \overline{w}_i f_i = \frac{\sum_i w_i f_i}{\sum_i w_i} \quad (12)$$

3.3. Least Squares Support Vector Machine (LSSVM)

LSSVM is a modification of the SVM algorithm to reduce the SVM's complexity of reaching the solutions [59–61,70–76]. LSSVM was firstly proposed by Suykens and Vandewalle [71] in 1999. In the SVM algorithm, a maximum separation plane is formed through mapping the input spaces into multi-dimensional possible regions using a specified function [71,72,77]. SVM algorithm's specific formulation provides the possibility of applying both linear and non-linear regressions to solve the problem.

Preprints (www.preprints.org) | NOT PEER-REVIEWED | Posted: 9 July 2019 doi:10.20944/preprints201907.0129.v1

Consider a given set of experimental data points as $\{(x_1,y_1), (x_2,y_2), \ldots, (x_N,y_N)\}$, where N, $x_i \in R^n$ and $y_i \in R$ represent the total number of data points, input data, and output data, respectively. The SVM formulation for such dataset is given as follows:

$$y = w^T \varphi(x) + b \tag{2}$$

where, w, $\varphi(x)$, T, and b denote weight vector, a non-linear function, transposed vector, and bias, respectively. The regression problem is subjected to the following constraints if the dataset could be separated into two classes [71,74,75]:

$$\begin{cases} w^T.\varphi(x_i) + b \geq 1 & if\ y = +1 \\ w^T.\varphi(x_i) + b \leq -1 & if\ y = -1 \end{cases} \tag{3}$$

Equation (4) represents an equivalent form of the above-mentioned constraints. However, Cortes and Vapnik [78] proposed the constraints for non-separable cases (Eq. (5)) by defining the slack variables that are positive or equal to zero parameters (Eq. (6)).

$$y_i[w^T.\varphi(x_i) + b] \geq +1 \quad , \quad i = 1,2,3,\ldots,N \tag{4}$$

$$y_i[w^T.\varphi(x_i) + b] \geq 1 - \xi_i \quad , \quad i = 1,2,3,\ldots,N \tag{5}$$

$$\xi_i \geq 0 \quad , \quad i = 1,2,3,\ldots,N \tag{6}$$

The following cost function has to be optimized regarding the constraints given in Eq. (4).

$$Cost\ function = \frac{1}{2} w^T w + \frac{C}{2} \sum_{i=1}^{N} \xi_i^p \tag{7}$$

Where C, a real positive number, represents a balanced value between the minimum and the maximum possible classification error. The results of the optimization process subjected to a set of specified constraints is achieved by employing the Lagrangian saddle point with Lagrangian multipliers α and β.

Preprints (www.preprints.org) | NOT PEER-REVIEWED | Posted: 9 July 2019 doi:10.20944/preprints201907.0129.v1

$$U(w,b,\alpha,\xi,\beta)=\frac{1}{2}w^Tw+\frac{C}{2}\sum_{i=1}^{N}\xi_i-\sum_{i=1}^{N}\alpha_i\,(y_i[w^T.\varphi(x_i)+b]-1+\xi_i)-\sum_{i=1}^{N}\beta_i\xi_i \quad (8)$$

As mentioned earlier, the LSSVM utilizes a linear set of equations to solve the regression problem instead of the quadratic programming applied in the SVM algorithm. LSSVM introduces a new cost function (Eq. 9) subjected to the equality constraint, Eq. 10.

$$cost\ function=\frac{1}{2}ww^T+\frac{\gamma}{2}\sum_{i=1}^{N}\xi_i^2 \quad (9)$$

$$y_i[w^T.\varphi(x_i)+b]=1-\xi_i \quad , \quad i=1,2,3,\dots,N \quad (10)$$

where γ and ξ_i represent the tuning parameter and regression error, respectively. γ equilibrates the training error and complexity of the model.

The following Lagrangian function is applied to determine the optimum solution:

$$U(w,b,\alpha,\xi)=\frac{1}{2}w^Tw+\frac{\gamma}{2}\sum_{i=1}^{N}\xi_i^2-\sum_{i=1}^{N}\alpha_i\,(y_i[w^T.\varphi(x_i)+b]-1+\xi_i) \quad (11)$$

The Lagrangian multiplier, α, would have either positive or negative values based on LSSVM formulation. Equating the differentiation of the Eq. (11) with respect to w, b, ξ, and α to zero leads to the determination of the optimum solution [71,79].

$$\begin{cases}\frac{\partial U}{\partial w}=0\Longrightarrow w=\sum_{i=1}^{N}\alpha_i y_i\varphi(x_i)\\ \frac{\partial U}{\partial b}=0\Longrightarrow\sum_{i=1}^{N}\alpha_i y_i=0\\ \frac{\partial U}{\partial \xi_i}=0\Longrightarrow\alpha_i=\gamma\xi_i\ ,\ i=1,2,\dots,N\\ \frac{\partial U}{\partial \alpha_i}=0\Longrightarrow y_i[w^T\varphi(x_i)+b]=1-\xi_i\ ,\quad i=1,2,\dots,N\end{cases} \quad (12)$$

Karnush-Kuhn-Trucker equation is given by Eq. (13). In this equation, $Y=[y_1,y_2,\dots,y_N]^T$, $\alpha=[\alpha_1,\alpha_2,\dots,\alpha_N]^T$, $1=[1,1,\dots,1]^T$, Ω and I_N denote the $N\times N$ kernel and identity matrices, respectively [71,79]. The Karnush-Kuhn-Trucker equation eliminates ξ and w parameters.

Preprints (www.preprints.org) | NOT PEER-REVIEWED | Posted: 9 July 2019 doi:10.20944/preprints201907.0129.v1

$$\begin{bmatrix} 0 & 1_N^T \\ 1_N & \Omega + \gamma^{-1} I_N \end{bmatrix} \begin{bmatrix} b \\ \alpha \end{bmatrix} = \begin{bmatrix} 0 \\ y \end{bmatrix} \quad (13)$$

SVM and LSSVM algorithms imply the kernel function in their formulation. Different kernel functions are available to be applied to the formulation. RBF type kernel function given by Eq. (14) is applied in this study where σ^2 represents the Gaussian function's squared variance, which has to be minimized in the SVM.

$$K(x_i, x_j) = exp\left(-\frac{\|x_i - x_k\|^2}{\sigma^2}\right) \quad (14)$$

Regarding the inclusion of the RBF in LSSVM, there are two parameters to be tuned during model development, e.g. γ and σ^2. Parameters tuning is carried out by minimizing the deviation of predicted values and obtained data form experiment. The mean square error determines such a deviation:

$$MSE = \frac{\sum_{i=1}^{N}\left(kr_{pred_i} - kr_{pred_j}\right)^2}{N} \quad (15)$$

Where k_r represents the relative permeability of oil, and pred and exp subscripts represent the experimental and estimated values of the permeability, respectively. The coupled simulated annealing optimization method is associated with the LSSVM formulation based on the flow chart presented in **Figure 3**.

4. Results and Discussions

The proposed MLP-ANN, ANFIS, and LSSVM strategies were associated with common optimization algorithms such as Levenberg Marquardt, particle swarm optimization (PSO), simulated annealing (SA). Training results of the MLP-ANN associated with Levenberg Marquardt optimization method is given in **Figure 4**, where the plot of mean square error versus

Preprints (www.preprints.org) | NOT PEER-REVIEWED | Posted: 9 July 2019 doi:10.20944/preprints201907.0129.v1

different epochs/iterations is illustrated. The detailed information of MLP-ANN including the number of hidden and output layer are also listed in **Table 2**. Particle swarm optimization (PSO) method is utilized in association with ANFIS strategy to determine optimum parameters. The trained membership functions are also depicted in **Figure 5** for each input parameters. Detailed information about the proposed ANFIS model is reported in **Table 3**. Two kind of tuning parameters (γ and σ^2) were used in the LSSVM machine. The optimized values for γ and σ^2 are 246882.356 and 0.8642, respectively.

4.1. Model Accuracy

We applied both graphical and statistical approaches to evaluate the models' performances regarding the estimation of the k_{ro}. **Figure 6** illustrates the cross plot of the predicted values versus experimental values. The majority of data points for both training and testing datasets are concentrated around the Y=X line which implies the accurate predictions of the proposed models. **Figure 7** plots the deviation plot of the proposed models. As is demonstrate in figures, the deviation of relative permeability increases as the relative permeation tends towards zero. Mathematically, This could be described as follows; as the dominator of the ratio becomes smaller and smaller, the results of the simulation will show higher levels of k_{ro} and leads in an infinite value of the relative error.. Hence, such experimental data points have been eliminated prior to plotting this figure. The relative deviation of the majority of data points ranges between -10% and +10% for k_{ro}. **Figure 8** illustrates the absolute deviation plot. The absolute deviation may lead to some misunderstandings about experimental values near zero. For instance, assume a deviation equal to 0.05 for experimental values of 0.1 and 1.0. The former represents a 50% error while the latter only represent 5% error. Thus, the absolute deviation measurement may give a false interpretation of the model performance in lower experimental values.

Preprints (www.preprints.org) | NOT PEER-REVIEWED | Posted: 9 July 2019 doi:10.20944/preprints201907.0129.v1

Statistical parameters were also applied to evaluate the models' accuracy. These parameters are relative mean square error (RMSE), average relative deviation (ARD), average absolute relative deviation (AARD), and coefficient of determination (R^2) and are formulated as follows:

$$RMSE = \left(\frac{1}{N}\sum_{i=1}^{N}\left(y_i^{pred.} - y_i^{exp.}\right)^2\right)^{0.5} \quad (16)$$

$$ARD = \frac{100}{N}\sum_{i=1}^{N}\left(\frac{y_i^{pred.} - y_i^{exp.}}{y_i^{exp.}}\right) \quad (17)$$

$$AARD = \frac{100}{N}\sum_{i=1}^{N}\left(\left|\frac{y_i^{pred.} - y_i^{exp.}}{y_i^{exp.}}\right|\right) \quad (18)$$

$$R^2 = 1 - \frac{\sum_{i=1}^{N}\left(y_i^{pred.} - y_i^{exp.}\right)^2}{\sum_{i=1}^{N}\left(y_i^{pred.} - \bar{y}^{exp.}\right)^2} \quad (19)$$

These parameters are reported for different set of data in **Table 4**. The coefficient of determination (R^2) indicates how close predicted values are to experimental values. This parameter usually lies between 0 and 1.0. Closer values to unity indicate more accurate predictions. Near unity coefficients of determination for proposed models, represent their capability in predicting the k_{ro}. RMSE and AARD also indicate the good performance of the proposed models. Cumulative frequency of the k_{ro} is also plotted in **Figure 9** which indicates the number of data points that have been predicted within a specified ARD range, e.g. less than 10%. The cumulative frequency figures indicate that 70%,67%, and 82% of the predicted data points are within 10% absolute relative deviation for MLP-ANN, ANFIS, and LSSVM, respectively. Considering both graphical and statistical error analyses, the proposed models can be considered as reliable predictive tools for k_{ro} estimations.

4.2. Model Validation

Preprints (www.preprints.org) | NOT PEER-REVIEWED | Posted: 9 July 2019 doi:10.20944/preprints201907.0129.v1

The proposed models are validated to see how they follow known trends. On the other hand it must be noted that the responses of derived models to the saturation of water, viscosities of oil and water could be determined but they cannot be judged, since effects of such parameters on the permeability are not completely known. But, it can be said that the k_{ro} reduces due to increasing of S_w. The proposed models follow such a trend, thus the rule is applicable to for the entire set of data. The simultaneous plot of experimental and predicted versus data index is depicted in **Figure 10**.

4.3. Outlier Detection

Experimental data points always associated with uncertainties. In case of k_{ro} measurements, when effects of scaling coefficients or some dimensionless numbers are not considered [80,81], the uncertainties will effectively affect any k_{ro} models based on such experimental data points. The outlier detection performed with the aim of determination of data points that show considerable deviations from the majority of data points [82]. The leverage value procedure applied as an outlier detection method in this study [83–85]. This approach consists of two numerical and graphical evaluations. At first, the Hat and the residual values of any input were calculated. The following formulation applied to calculate the Hat matrix:

$$H = X(X^T X)^{-1} X^T \quad (20)$$

X is a matrix of size $N \times P$, where N represents the total number of data points and P denotes the number of input parameters. T and -1 are transposed and inverse operators, respectively. The standardized residual value of each data point calculated and employed to plot standardized values versus hat values, called Williams plot. A warning leverage value is also defined using the following expression:

Preprints (www.preprints.org) | NOT PEER-REVIEWED | Posted: 9 July 2019 doi:10.20944/preprints201907.0129.v1

$$H^* = \frac{3(P+1)}{N} \quad (21)$$

A rectangular area restricted to $R=\pm 3$ and $0 \leq H \leq H^*$ is considered as the feasible region. The model is considered as reliable if the majority of data points are located in the feasible region. Williams plot of the proposed models is illustrated in **Figure 11**. As you can see, the majority of data points located inside the feasible region. However, there are some data points outside the restricted area. Data points with hat values greater than the warning leverage and standardized residual $-3 \leq R \leq +3$ are called the "high good leverage" since they haven't any effect on the value of R-squared. However, data points with standardized residual values less than -3 or greater than +3 are considered "bad leverage".

4.4. Sensitivity Analysis

A sensitivity analysis was carried out to find out how each input parameter affects the target variable, namely the k_{ro}. Quantitative effect of each parameter calculated using Pearson's method [86] and a relevancy factor defined by the following expression:

$$r = \frac{\sum_{i=1}^{N}(X_{k,i}-\bar{X}_k)(y_i-\bar{y})}{\sqrt{\sum_{i=1}^{N}(X_{k,i}-\bar{X}_k)^2 \sum_{i=1}^{N}(y_i-\bar{y})^2}} \quad (22)$$

where N, $X_{k,i}$, Y_i, $\bar{X}_k$, $\bar{Y}$ are the total number of data points, i^{th} input value of the k^{th} parameter, i^{th} output value, average value of the k^{th} input parameter, and mean value of the output parameter, respectively. The relevancy factor lays between -1 and +1 which higher absolute values represent the higher effect of the corresponding parameter. Positive effect reflects the target variable's increment as a specific input parameter increases, while the negative effect reflects the target variable's decrement as a specific input parameter increases. **Figure 12** illustrates the sensitivity analysis results, which S_w had the highest negative effects with relevancy factor of -0.72.

Preprints (www.preprints.org) | NOT PEER-REVIEWED | Posted: 9 July 2019 doi:10.20944/preprints201907.0129.v1

4.5. Models Comparison

The proposed MLP-ANN, ANFIS, and LSSVM strategies are compared to four well-known models, namely Bennion et al. [18], Mosavat et al. [57], Torabi et al. [56], Zhang et al. [58] , and Esmaeili et al. models [48]. These models are listed in **Table 5**.

Figure 13 represents the statistical analyses of previously reported k_{ro} models. Bennion et al. [18] proposed the most simple model. This model consists of two temperature ranges, $60℃<T<100℃$ and $150℃<T<275℃$.. For experimental data points measured in temperatures ranging from 100 to $150℃$, the average value of the two correlation proposed by Bennion et al. employed. This model also underestimates the experimental values leading to the negative ARD values for k_{ro} predictions. Mosavat et al. model [57], overestimated majority of data points and had less accurate predictions for k_{ro} regarding the calculated coefficient of determination. Torabi et al. [56] model showed unacceptable performance since considerable deviations from experimental data points observed for the predicted values. Finally, Esmaeili et al.'s model [48] performance is evaluated, showing the best performance among the previously reported models and has the highest calculated coefficient of determination. Hence, comparing the results of the proposed MLP-ANN, ANFIS, and LSSVM strategies indicate the better performance of these models and their capability of predicting the k_{ro}.

5. Conclusion

Three new models were proposed to forecast the K_{ro} in a sandstone reservoir in various temperatures. These models utilized the MLP-ANN network, ANFIS approach and LSSVM to link the k_{ro} to the corresponding input parameters, i.e. S_w, μ_o, , μ_w, and temperature. The total dataset applied to develop new model comprised of 626 data points. R-squared and AARD values

of 0.985 and 22.47%, 0.975 and 28.02%, and 0.999 and 8.33% were observed for MLP-ANN, ANFIS, and LSSVM models, respectively. The comparative study also indicated that the proposed models had better performance than previously reported permeability models. However, the LSSVM model had the best performance regarding the graphical and statistical error analyses.

References

[1] Wang Y, Ren S, Zhang L, Peng X, Pei S, Cui G, et al. Numerical study of air assisted cyclic steam stimulation process for heavy oil reservoirs: Recovery performance and energy efficiency analysis. Fuel 2018;211:471–83.

[2] Rui Z, Wang X, Zhang Z, Lu J, Chen G, Zhou X, et al. A realistic and integrated model for evaluating oil sands development with steam assisted gravity drainage technology in Canada. Appl Energy 2018;213:76–91.

[3] Wang Z, Gu S. State-of-the-art on the development of ultrasonic equipment and key problems of ultrasonic oil prudction technique for EOR in China. Renew Sustain Energy Rev 2018;82:2401–7.

[4] Mokheimer EMA, Hamdy M, Abubakar Z, Shakeel MR, Habib MA, Mahmoud M. A Comprehensive Review of Thermal Enhanced Oil Recovery: Techniques Evaluation. J Energy Resour Technol 2019;141:30801.

[5] Edmondson TA. Effect of temperature on waterflooding. J Can Pet Technol 1965;4:236–42.

[6] Davidson LB. The effect of temperature on the permeability ratio of different fluid pairs in two-phase systems. J Pet Technol 1969;21:1–37.

[7] Poston SW, Ysrael S, Hossain A, Montgomery III EF. The effect of temperature on irreducible water saturation and relative permeability of unconsolidated sands. Soc Pet Eng J 1970;10:171–80.

[8] Maini BB, Okazawa T. Effects of temperature on heavy oil-water relative permeability of sand. J Can Pet Technol 1987;26.

[9] Maini BB, Batycky JP. Effect of temperature on heavy-oil/water relative permeabilities in horizontally and vertically drilled core plugs. J Pet Technol 1985;37:1–500.

[10] Esfahani MR, Haghighi M. Wettability evaluation of Iranian carbonate formations. J Pet Sci Eng 2004;42:257–65.

[11] Amott E. Observations relating to the wettability of porous rock 1959.

[12] Anderson WG. Wettability literature survey-part 3: the effects of wettability on the electrical properties of porous media. J Pet Technol 1986;38:1–371.

[13] Polikar M, Ferracuti F, Decastro V, Puttagunta R, Ali SM. Effect of temperature on bitumen-water end point relative permeabilities and saturations. J Can Pet Technol 1986;25.

[14] Polikar M, Ali SM, Puttagunta VR. High-temperature relative permeabilities for Athabasca oil sands. SPE Reserv Eng 1990;5:25–32.

[15] Ashrafi M, Souraki Y, Torsaeter O. Investigating the temperature dependency of oil and water relative permeabilities for heavy oil systems. Transp Porous Media 2014;105:517–37.

[16] Ashrafi M, Souraki Y, Torsaeter O. Effect of Temperature on Athabasca Type Heavy Oil–Water Relative Permeability Curves in Glass Bead Packs. Energy Environ Res 2012;2:113.

[17] Weinbrandt RM, Ramey Jr HJ, Casse FJ. The effect of temperature on relative and absolute permeability of sandstones. Soc Pet Eng J 1975;15:376–84.

[18] Bennion DB, Thomas FB, Schulmeister B, Ma T. A Correlation of the Low and High Temperature Water-Oil Relative Permeability Characteristics of Typical Western Canadian Unconsolidated Bitumen Producing Formations. Can. Int. Pet. Conf., Petroleum Society of Canada; 2006.

[19] Li B, fen Pu W, xing Li K, Jia H, Wang KY, guang Yang Z. The Characteristics and Impacts Factors of Relative Permeability Curves in High Temperature and Low-Permeability Limestone Reservoirs. Adv Mater Res 2014.

[20] Lo HY, Mungan N. Effect of temperature on water-oil relative permeabilities in oil-wet and water-wet systems. Fall Meet. Soc. Pet. Eng. AIME, Society of Petroleum Engineers; 1973.

[21] Kumar M, Inouye TA. Low-temperature analogs of high-temperature water/oil relative permeabilities. SPE Annu. Tech. Conf. Exhib., Society of Petroleum Engineers; 1994.

[22] Kumar S, Torabzadeh SJ, Handy LL. Relative permeability functions for high-and low-tension systems at elevated temperatures. SPE Calif. Reg. Meet., Society of Petroleum Engineers; 1985.

[23] Schembre JM, Tang G, Kovscek AR. Effect of temperature on relative permeability for heavy-oil diatomite reservoirs. SPE West. Reg. Meet., Society of Petroleum Engineers; 2005.

[24] Sinnokrot AA, Ramey Jr HJ, Marsden Jr SS. Effect of temperature level upon capillary pressure curves. Soc Pet Eng J 1971;11:13–22.

[25] Sufi AH, Ramey Jr HJ, Brigham WE. Temperature effects on relative permeabilities of oil-water systems. SPE Annu. Tech. Conf. Exhib., Society of Petroleum Engineers; 1982.

[26] Akin S, Castanier LM, Brigham WE. Effect of temperature on heavy-oil/water relative permeabilities. SPE Annu. Tech. Conf. Exhib., Society of Petroleum Engineers; 1998.

[27] Bennion DW, Moore RG, Thomas FB. Effect of relative permeability on the numerical simulation of the steam stimulation process. J Can Pet Technol 1985;24.

[28] Closmann PJ, Waxman MH, Deeds CT. Steady-state tar/water relative permeabilities in Peace River cores at elevated temperature. SPE Reserv Eng 1988;3:76–80.

[29] Hamouda AA, Karoussi O. Effect of temperature, wettability and relative permeability on oil recovery from oil-wet chalk. Energies 2008;1:19–34.

[30] Hawkins JT. Comparison of three methods of relative permeability measurement. Log Anal 1989;30.

[31] Ehrlich R. The effect of temperature on water-oil imbibition relative permeability. SPE East. Reg. Meet., Society of Petroleum Engineers; 1970.

[32] Amaefule JO, Handy LL. The effect of interfacial tensions on relative oil/water permeabilities of consolidated porous media. Soc Pet Eng J 1982;22:371–81.

[33] Torabzadey SJ. The effect of temperature and interfacial tension on water/oil relative permeabilities of consolidated sands. SPE Enhanc. Oil Recover. Symp., Society of Petroleum Engineers; 1984.

[34] Baghban A, Ahmadi MA, Shahraki BH. Prediction carbon dioxide solubility in presence of various ionic liquids using computational intelligence approaches. J Supercrit Fluids

2015;98:50–64.

[35] Hosseini Nazhad SH, Sasanipour J, Parsaei MR, Javidan R, Baghban A. Estimating water content of natural gas: A radial basis function neural network method. Pet Sci Technol 2017;35. doi:10.1080/10916466.2017.1339198.

[36] Baghban A, Sasanipour J, Goodarzi AM. Evolving ANFIS model to estimate sweet natural gas water content. Pet Sci Technol 2017;35. doi:10.1080/10916466.2017.1337795.

[37] Vapnik VN. Statistical learning theory. J. vol. 3. Wiley, New York; 1998.

[38] Hann TH, Steurer E. Much ado about nothing? Exchange rate forecasting: Neural networks vs. linear models using monthly and weekly data. Neurocomputing 1996;10:323–39.

[39] Baylar A, Hanbay D, Batan M. Application of least square support vector machines in the prediction of aeration performance of plunging overfall jets from weirs. Expert Syst Appl 2009;36:8368–74.

[40] Chen T-S, Chen J, Lin Y-C, Tsai Y-C, Kao Y-H, Wu K. A novel knowledge protection technique base on support vector machine model for anti-classification. Electr. Eng. Control, Springer; 2011, p. 517–24.

[41] Übeyli ED. Least squares support vector machine employing model-based methods coefficients for analysis of EEG signals. Expert Syst Appl 2010;37:233–9.

[42] Rafiee-Taghanaki S, Arabloo M, Chamkalani A, Amani M, Zargari MH, Adelzadeh MR. Implementation of SVM framework to estimate PVT properties of reservoir oil. Fluid Phase Equilib 2013;346:25–32.

[43] Amendolia SR, Cossu G, Ganadu ML, Golosio B, Masala GL, Mura GM. A comparative

study of k-nearest neighbour, support vector machine and multi-layer perceptron for thalassemia screening. Chemom Intell Lab Syst 2003;69:13–20.

[44] Baghban A, Sasanipour J, Zhang Z. A new chemical structure-based model to estimate solid compound solubility in supercritical CO<inf>2</inf>. J CO2 Util 2018;26. doi:10.1016/j.jcou.2018.05.009.

[45] Arabloo M, Shokrollahi A, Gharagheizi F, Mohammadi AH. Toward a predictive model for estimating dew point pressure in gas condensate systems. Fuel Process Technol 2013;116:317–24. doi:https://doi.org/10.1016/j.fuproc.2013.07.005.

[46] Fayazi A, Arabloo M, Shokrollahi A, Zargari MH, Ghazanfari MH. State-of-the-art least square support vector machine application for accurate determination of natural gas viscosity. Ind Eng Chem Res 2013;53:945–58.

[47] Farasat A, Shokrollahi A, Arabloo M, Gharagheizi F, Mohammadi AH. Toward an intelligent approach for determination of saturation pressure of crude oil. Fuel Process Technol 2013;115:201–14.

[48] Esmaeili S, Sarma H, Harding T, Maini B. A data-driven model for predicting the effect of temperature on oil-water relative permeability. Fuel 2019;236:264–77. doi:https://doi.org/10.1016/j.fuel.2018.08.109.

[49] Burdine N. Relative permeability calculations from pore size distribution data. J Pet Technol 1953;5:71–8.

[50] Corey AT. The interrelation between gas and oil relative permeabilities. Prod Mon 1954;19:38–41.

[51] Sigmund PM, McCaffery FG. An improved unsteady-state procedure for determining the relative-permeability characteristics of heterogeneous porous media (includes associated papers 8028 and 8777). Soc Pet Eng J 1979;19:15–28.

[52] Honarpour M, Koederitz LF, Harvey AH. Empirical equations for estimating two-phase relative permeability in consolidated rock. J Pet Technol 1982;34:2–905.

[53] Purcell WR. Capillary pressures-their measurement using mercury and the calculation of permeability therefrom. J Pet Technol 1949;1:39–48.

[54] Timmerman EH. Practical reservoir engineering. PennWell Corporation; 1982.

[55] Fatt I, Dykstra H. Relative permeability studies. J Pet Technol 1951;3:249–56.

[56] Torabi F, Mosavat N, Zarivnyy O. Predicting heavy oil/water relative permeability using modified Corey-based correlations. Fuel 2016;163:196–204.

[57] Mosavat N, Mohsenzadeh A, Al-Wahaibi Y. Estimating Oil/Water Relative Permeability at SAGD Steam Chamber Edge. SPE Heavy Oil Conf. Exhib., Society of Petroleum Engineers; 2016.

[58] Zhang L, Tong J, Xiong Y, Zhao Y. Effect of temperature on the oil–water relative permeability for sandstone reservoirs. Int J Heat Mass Transf 2017;105:535–48.

[59] Wang J, Dong M, Asghari K. Effect of oil viscosity on heavy oil-water relative permeability curves. SPE/DOE Symp. Improv. Oil Recover., Society of Petroleum Engineers; 2006.

[60] Sola BS, Rashidi F, Babadagli T. Temperature effects on the heavy oil/water relative permeabilities of carbonate rocks. J Pet Sci Eng 2007;59:27–42.

[61] Kovscek AR, Vega B. Steady-state relative permeability measurements, temperature

dependency and a reservoir diatomite core sample evolution. SPE Annu. Tech. Conf. Exhib., Society of Petroleum Engineers; 2014.

[62] Hamouda AA, Karoussi O, Chukwudeme EA. Relative permeability as a function of temperature, initial water saturation and flooding fluid compositions for modified oil-wet chalk. J Pet Sci Eng 2008;63:61–72.

[63] Mohanraj M, Jayaraj S, Muraleedharan C. Applications of artificial neural networks for thermal analysis of heat exchangers–a review. Int J Therm Sci 2015;90:150–72.

[64] Zadeh LA. Information and control. Fuzzy Sets 1965;8:338–53.

[65] Safari H, Nekoeian S, Shirdel MR, Ahmadi H, Bahadori A, Zendehboudi S. Assessing the dynamic viscosity of Na–K–Ca–Cl–H2O aqueous solutions at high-pressure and high-temperature conditions. Ind Eng Chem Res 2014;53:11488–500.

[66] Zarei K, Atabati M, Moghaddary S. Predicting the heats of combustion of polynitro arene, polynitro heteroarene, acyclic and cyclic nitramine, nitrate ester and nitroaliphatic compounds using bee algorithm and adaptive neuro-fuzzy inference system. Chemom Intell Lab Syst 2013;128:37–48.

[67] Nikravesh M, Zadeh LA, Aminzadeh F. Soft computing and intelligent data analysis in oil exploration. vol. 51. Elsevier; 2003.

[68] Lee KH. First course on fuzzy theory and applications. vol. 27. Springer Science & Business Media; 2006.

[69] Jang J-SR, Sun C-T, Mizutani E. Neuro-fuzzy and soft computing; a computational approach to learning and machine intelligence 1997.

[70] Pelckmans K, Suykens JAK, Van Gestel T, De Brabanter J, Lukas L, Hamers B, et al. LS-SVMlab: a matlab/c toolbox for least squares support vector machines. Tutorial KULeuven-ESAT Leuven, Belgium 2002;142:1–2.

[71] Suykens JAK, Vandewalle J. Least squares support vector machine classifiers. Neural Process Lett 1999;9:293–300.

[72] Cristianini N, Shawe-Taylor J. An introduction to support vector machines and other kernel-based learning methods. Cambridge university press; 2000.

[73] Akhlaghinia M, Torabi F, Chan CW. Effect of temperature on two-phase relative permeabilities of heavy oil, water, carbon dioxide, and methane determined by displacement technique. Energy & Fuels 2013;27:1185–93.

[74] Shokrollahi A, Arabloo M, Gharagheizi F, Mohammadi AH. Intelligent model for prediction of CO2–reservoir oil minimum miscibility pressure. Fuel 2013;112:375–84.

[75] Gharagheizi F, Eslamimanesh A, Farjood F, Mohammadi AH, Richon D. Solubility parameters of nonelectrolyte organic compounds: determination using quantitative structure–property relationship strategy. Ind Eng Chem Res 2011;50:11382–95.

[76] Coats KH, Smart GT. Application of a regression-based EOS PVT program to laboratory data. SPE Reserv Eng 1986;1:277–99.

[77] Suykens JAK, Van Gestel T, De Brabanter J, De Moor B, Vandewalle J. Least Squares Support Vector Machines,(Tutorial IJCNN) 2003.

[78] Cortes C, Vapnik V. Support-vector networks. Mach Learn 1995;20:273–97.

[79] Suykens JAK, Van Gestel T, DBJ B. De Moor, and J. Vandewalle. Least Squares Support

Vector Mach 2002.

[80] Peters EJ, Flock DL. The onset of instability during two-phase immiscible displacement in porous media. Soc Pet Eng J 1981;21:249–58.

[81] Rapoport LA, Leas WJ. Properties of Linear Waterfloods. J Pet Technol 1953;5:139–48. doi:10.2118/213-G.

[82] Rousseeuw PJ, Leroy AM. Robust regression and outlier detection. vol. 589. John wiley & sons; 2005.

[83] Gramatica P. Principles of QSAR models validation: internal and external. Mol Inform 2007;26:694–701.

[84] Goodall CR. 13 Computation using the QR decomposition. Handb Stat 1993;9:467–508.

[85] Mohammadi AH, Eslamimanesh A, Gharagheizi F, Richon D. A novel method for evaluation of asphaltene precipitation titration data. Chem Eng Sci 2012;78:181–5.

[86] Chok NS. Pearson's versus Spearman's and Kendall's correlation coefficients for continuous data 2010.

Preprints (www.preprints.org) | NOT PEER-REVIEWED | Posted: 9 July 2019 doi:10.20944/preprints201907.0129.v1

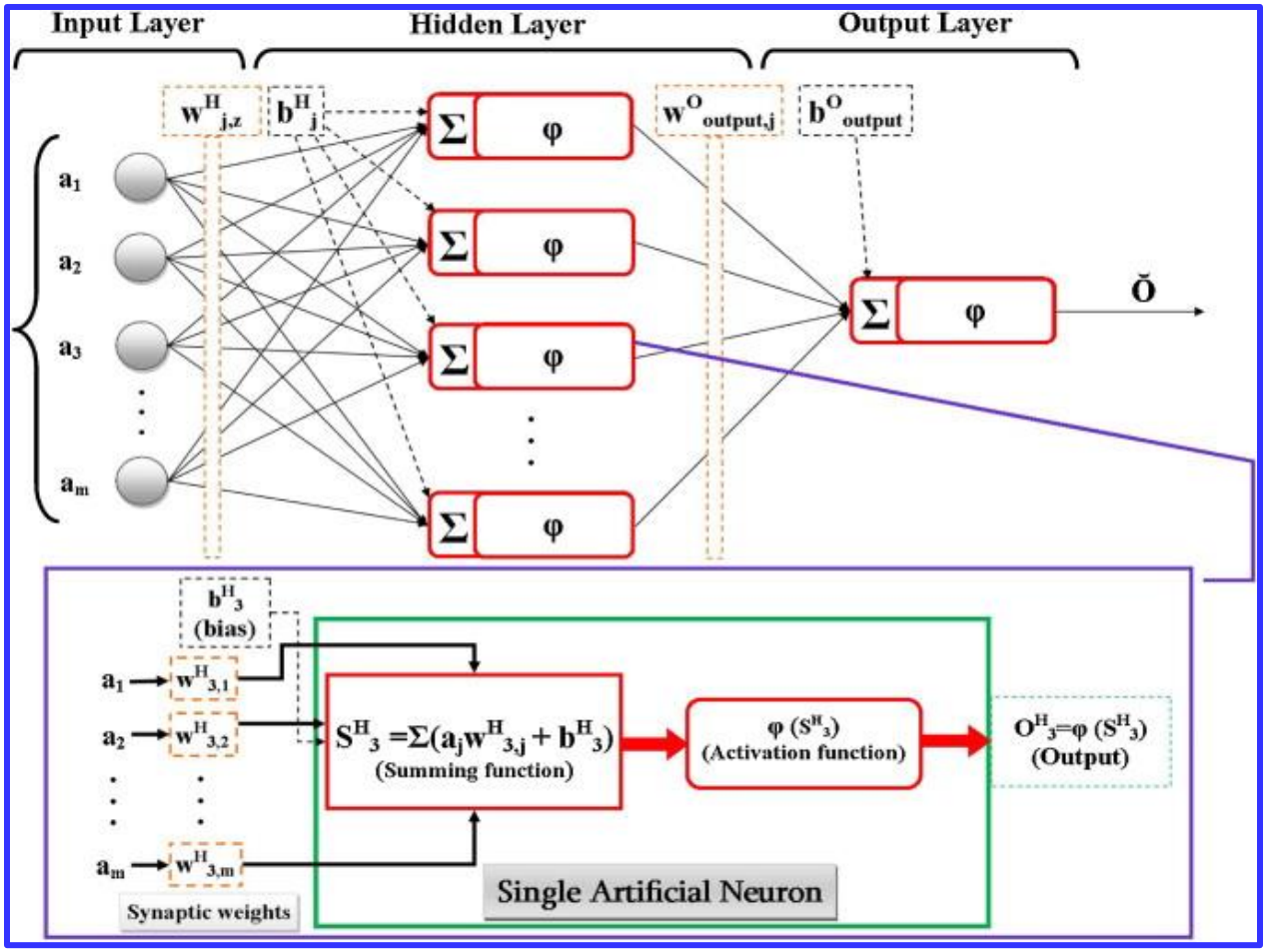

Figure 1. Schematic structure of a multilayer perceptron artificial neural network

Preprints (www.preprints.org) | NOT PEER-REVIEWED | Posted: 9 July 2019 doi:10.20944/preprints201907.0129.v1

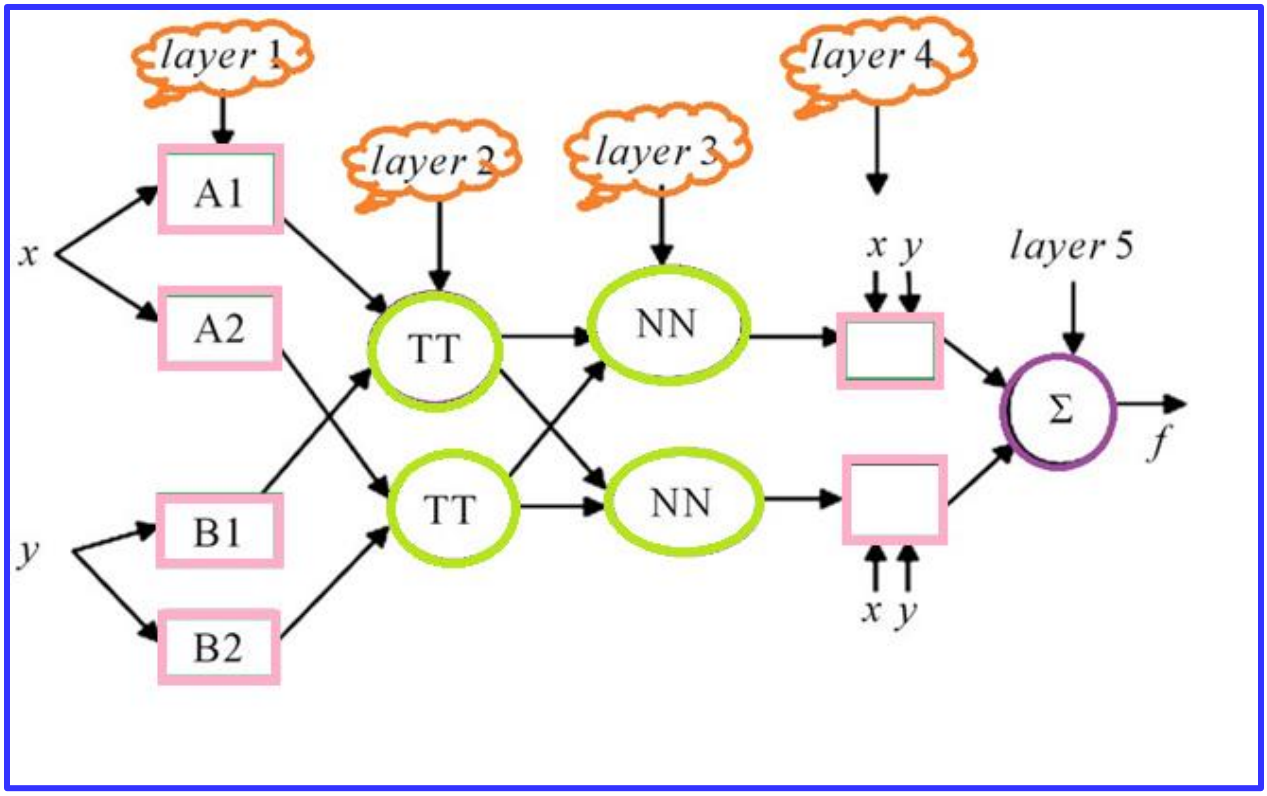

Figure 2. Overview of an ANFIS model.

Preprints (www.preprints.org) | NOT PEER-REVIEWED | Posted: 9 July 2019 doi:10.20944/preprints201907.0129.v1

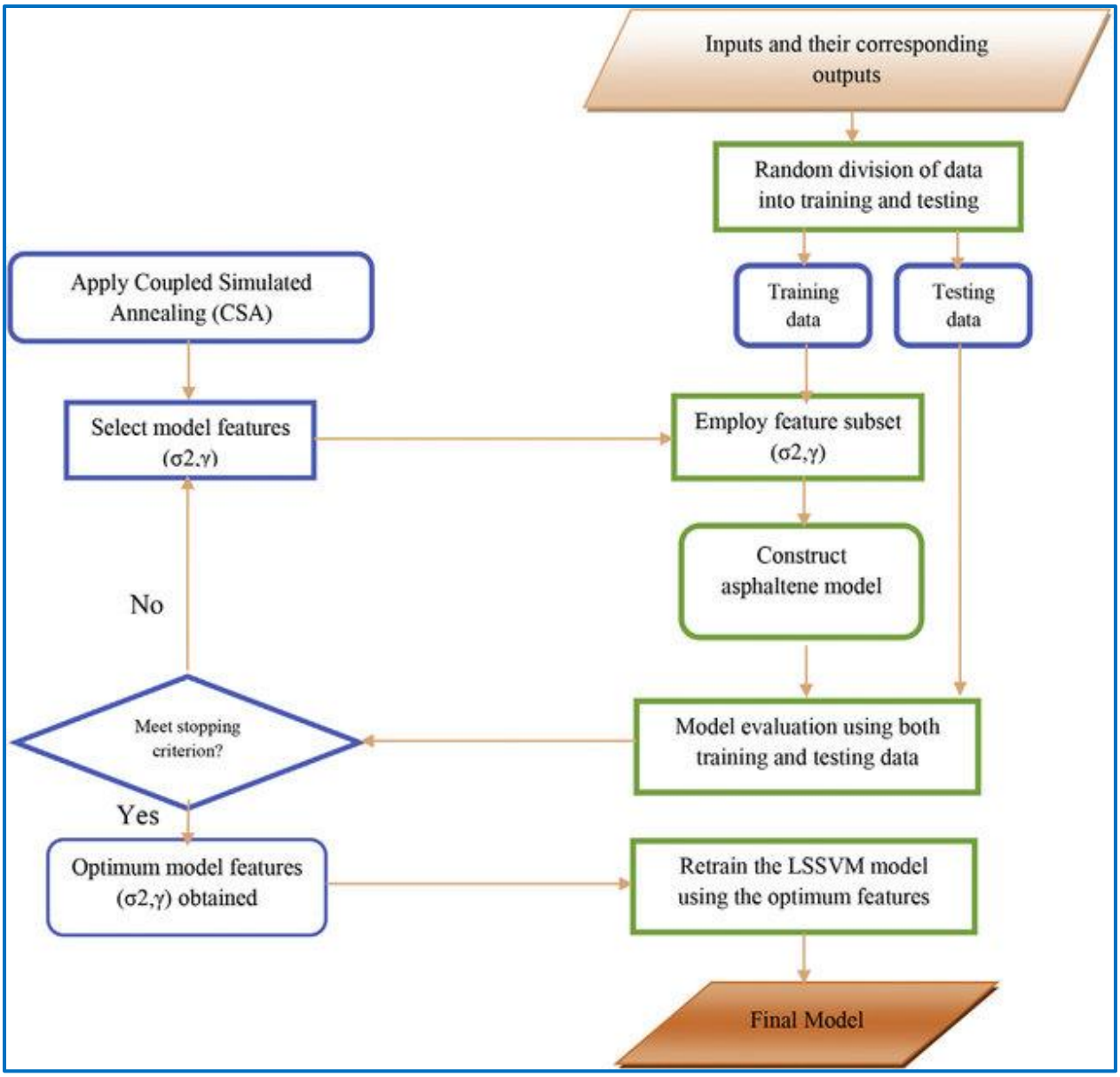

Figure 3. Flow chart of the LSSVM approach associated with coupled simulated annealing

Preprints (www.preprints.org) | NOT PEER-REVIEWED | Posted: 9 July 2019 doi:10.20944/preprints201907.0129.v1

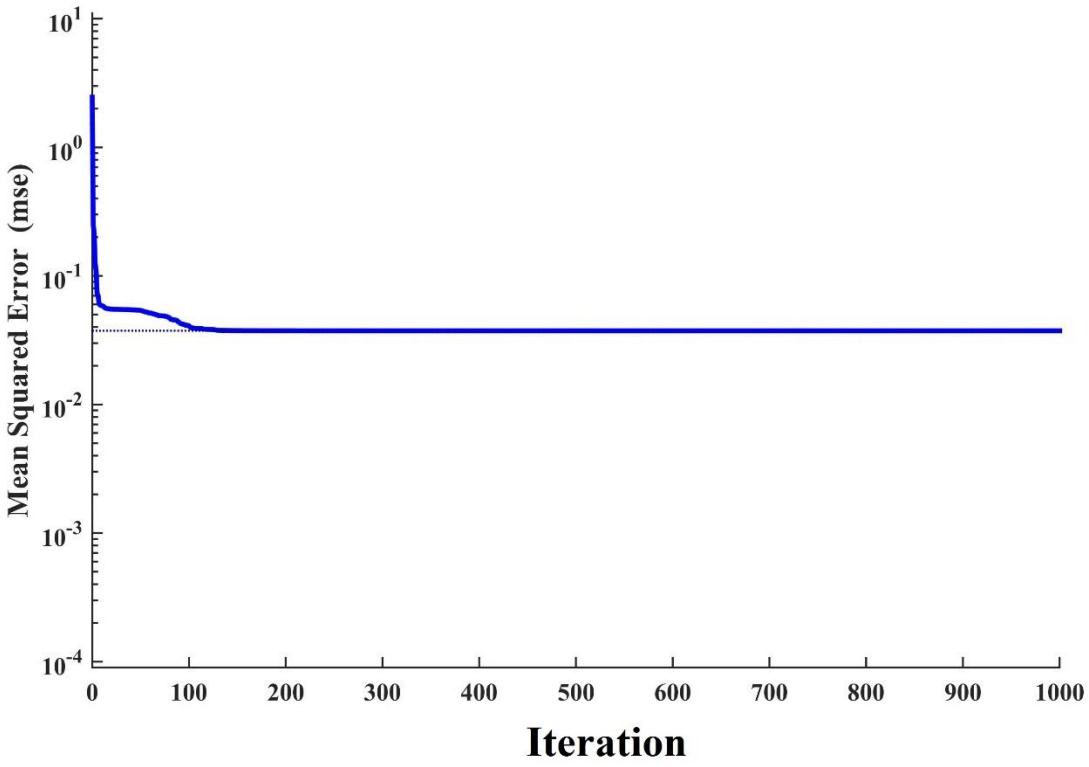

Figure 4. Levenberg Marquardt performance in training the multilayer perceptron artificial neural network.

Preprints (www.preprints.org) | NOT PEER-REVIEWED | Posted: 9 July 2019 doi:10.20944/preprints201907.0129.v1

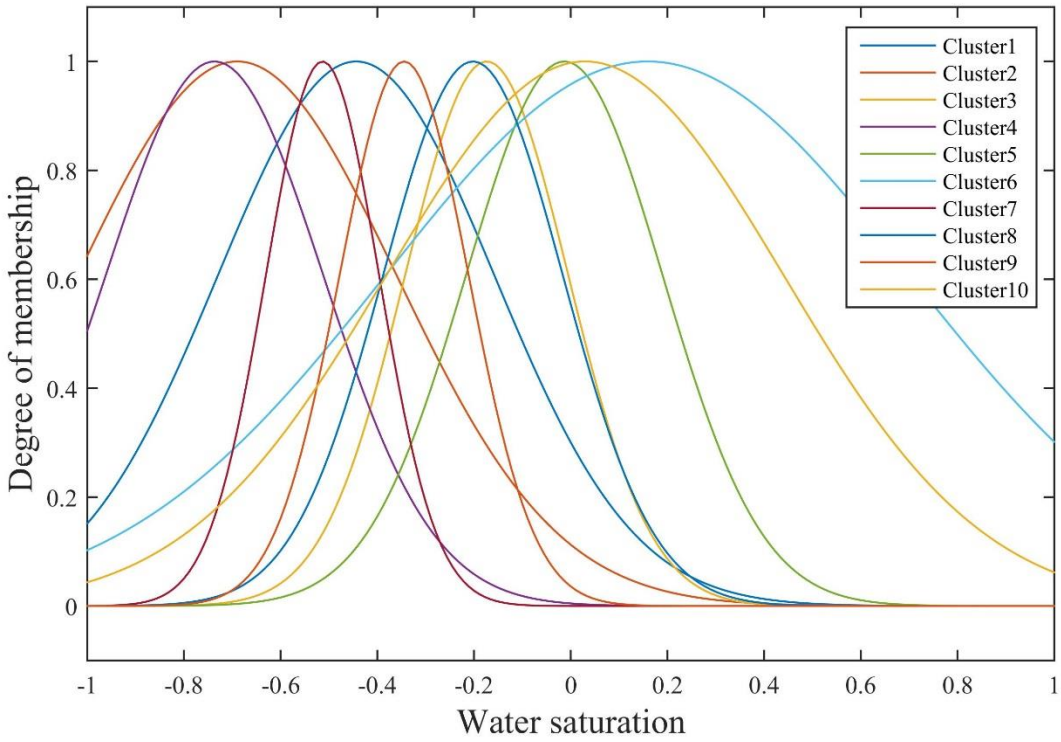

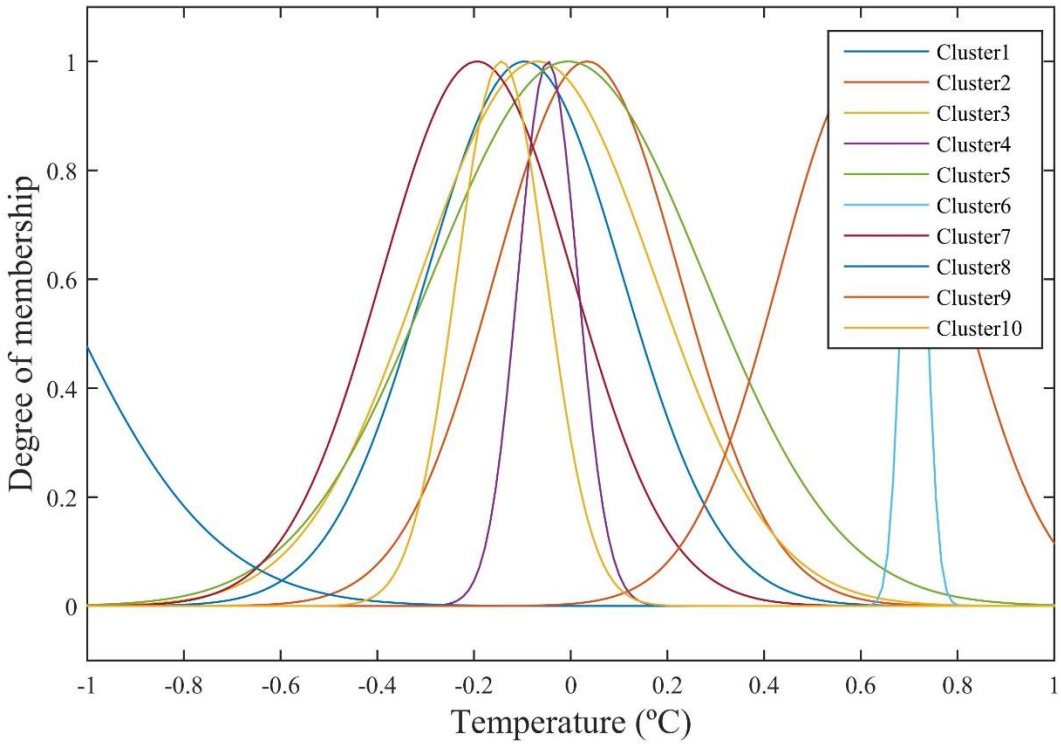

Preprints (www.preprints.org) | NOT PEER-REVIEWED | Posted: 9 July 2019 doi:10.20944/preprints201907.0129.v1

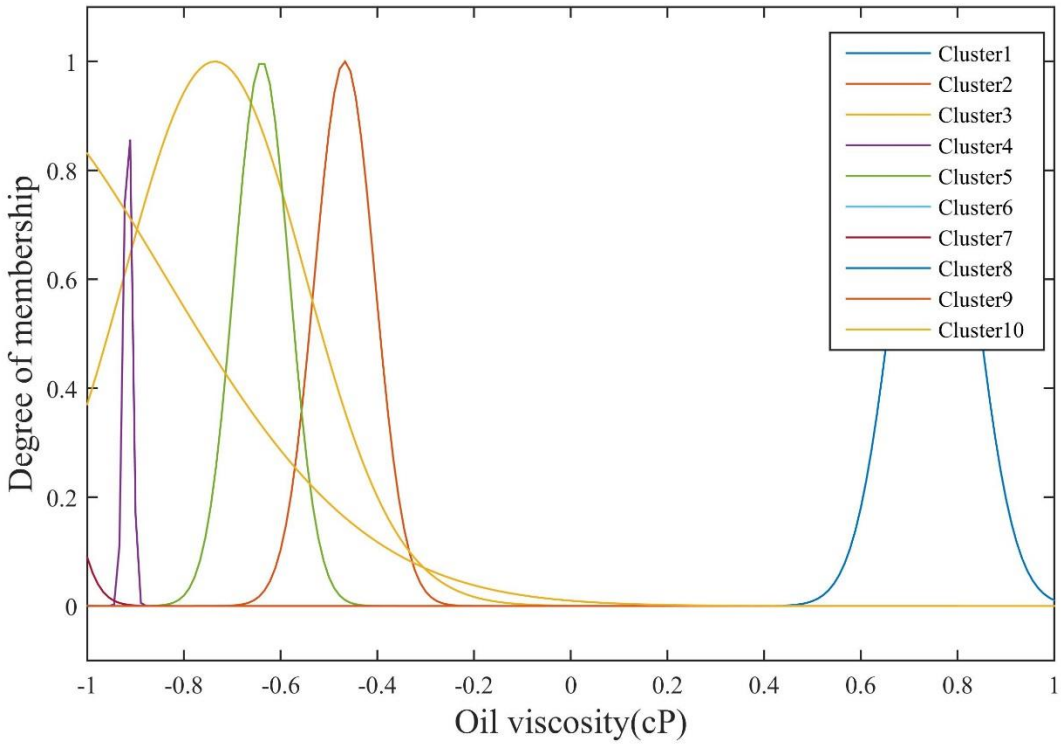

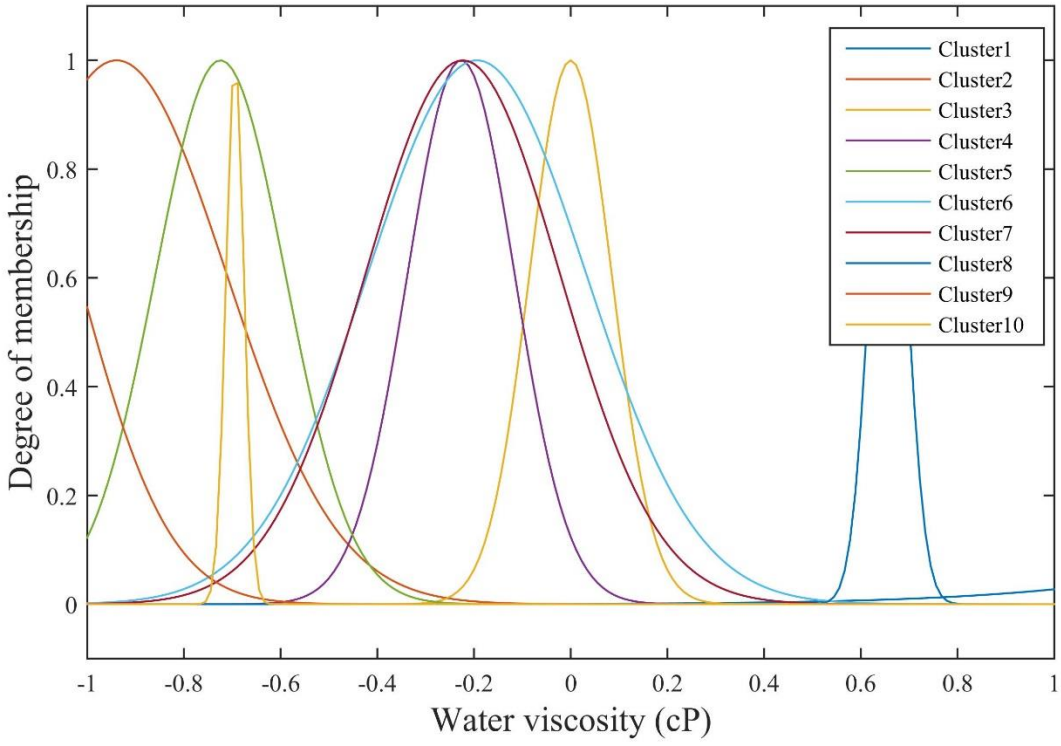

Preprints (www.preprints.org) | NOT PEER-REVIEWED | Posted: 9 July 2019 doi:10.20944/preprints201907.0129.v1

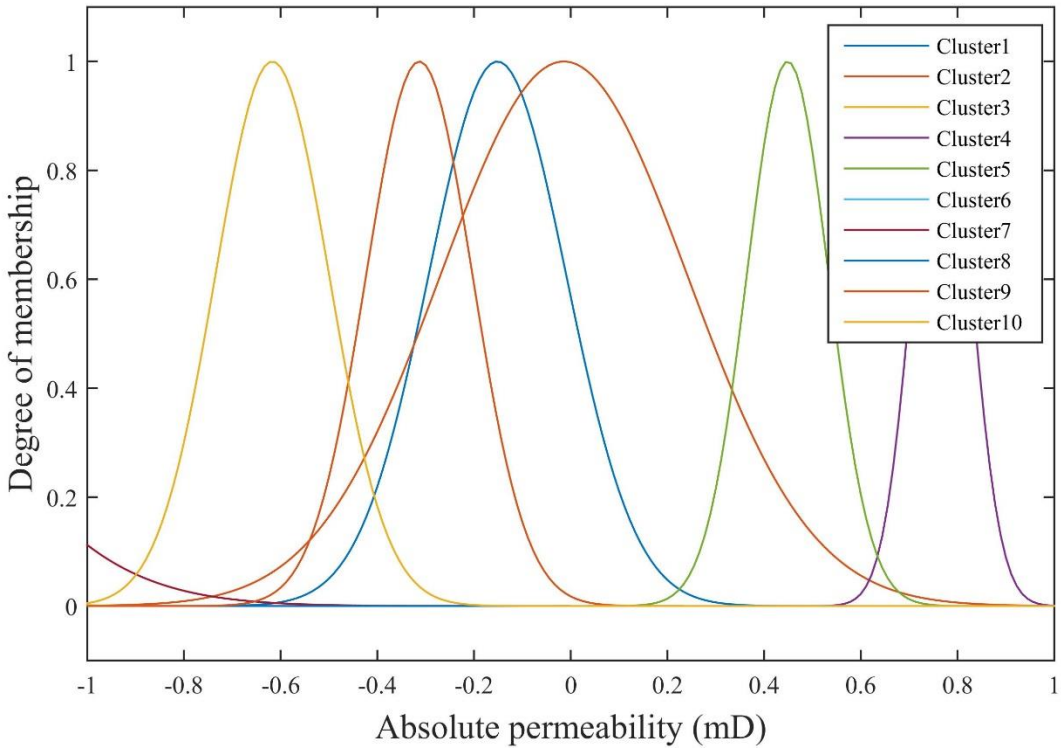

Figure 5. Trained membership functions for different variables.

Preprints (www.preprints.org) | NOT PEER-REVIEWED | Posted: 9 July 2019 doi:10.20944/preprints201907.0129.v1

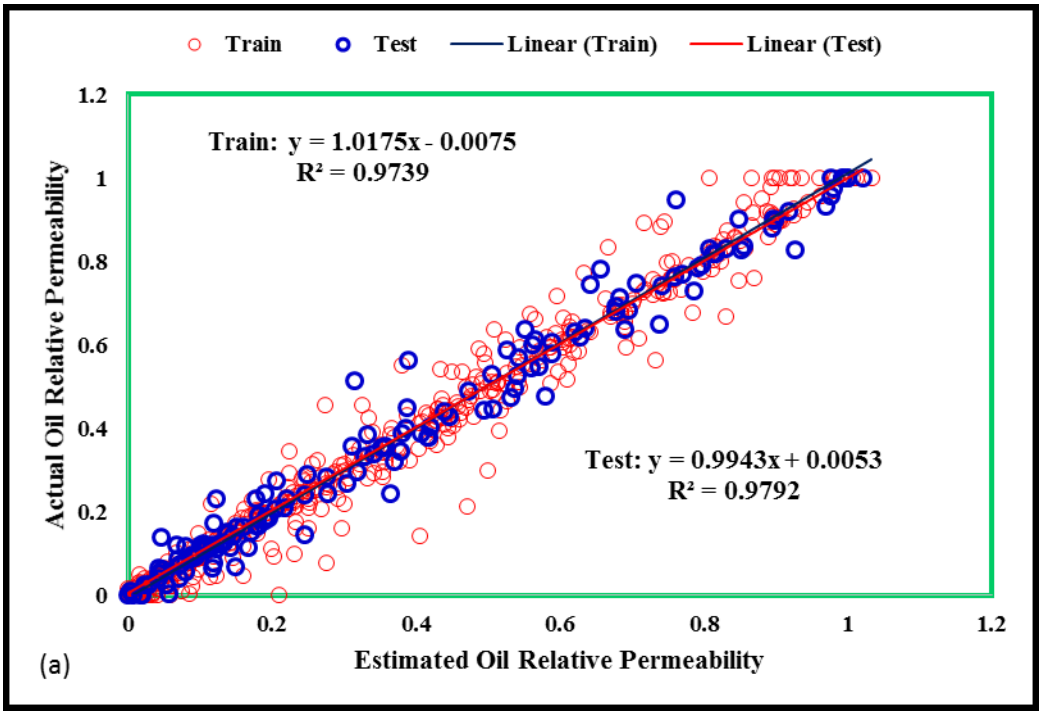

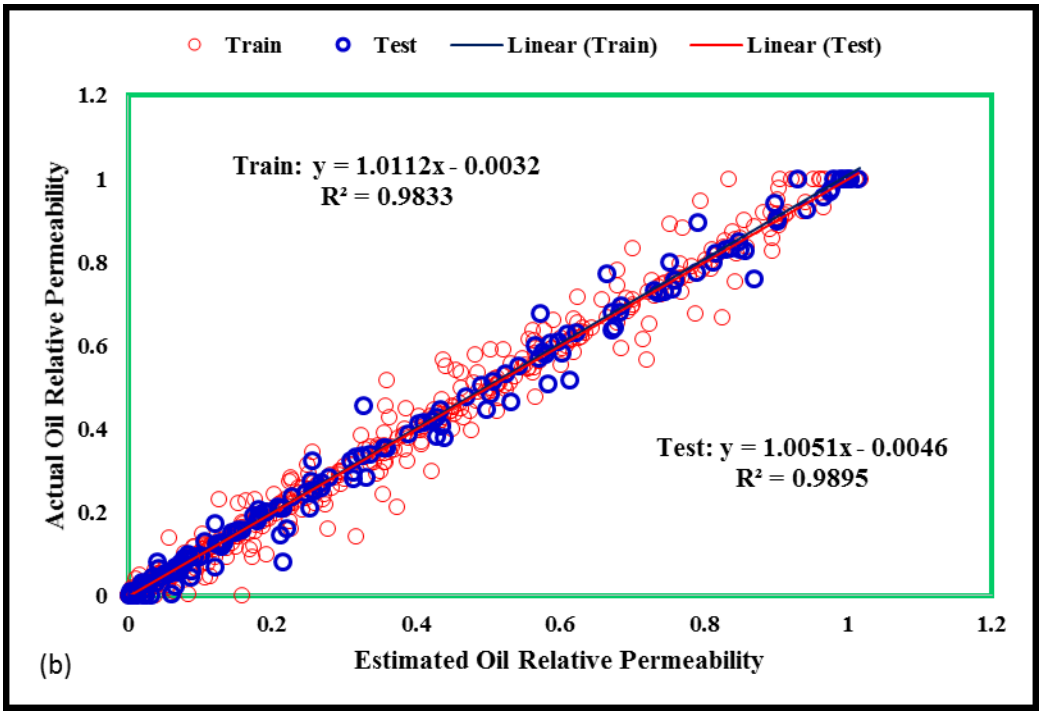

Preprints (www.preprints.org) | NOT PEER-REVIEWED | Posted: 9 July 2019 doi:10.20944/preprints201907.0129.v1

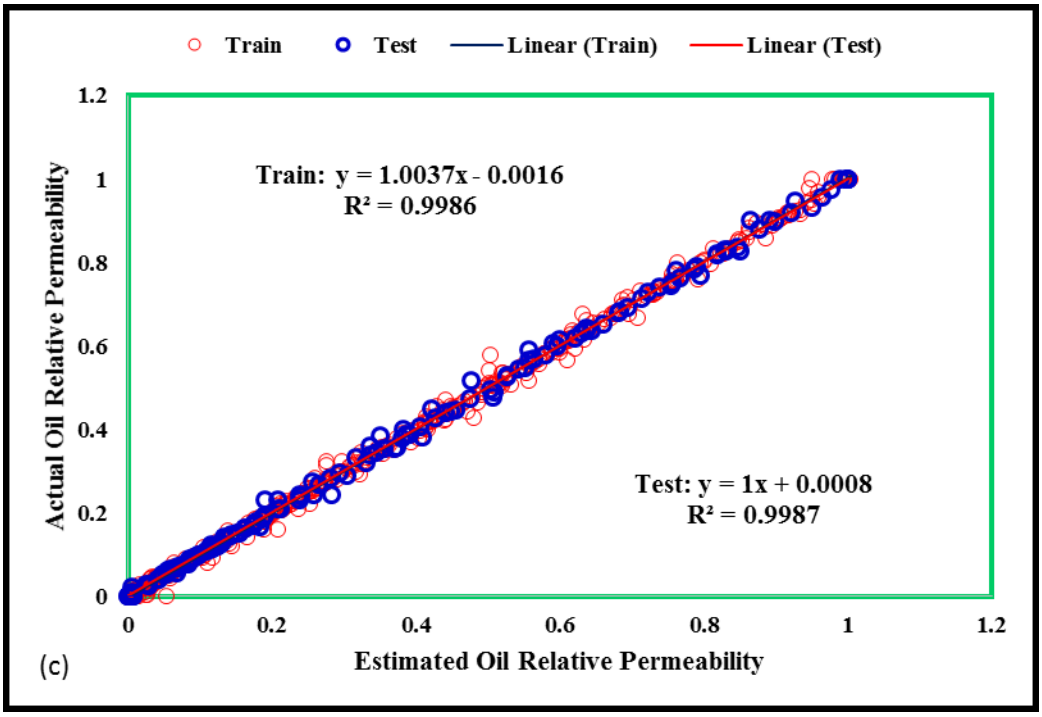

Figure 6. Cross plot of data points for: (a) ANFIS, (b) MLP-ANN, and (c) LSSVM.

Preprints (www.preprints.org) | NOT PEER-REVIEWED | Posted: 9 July 2019 doi:10.20944/preprints201907.0129.v1

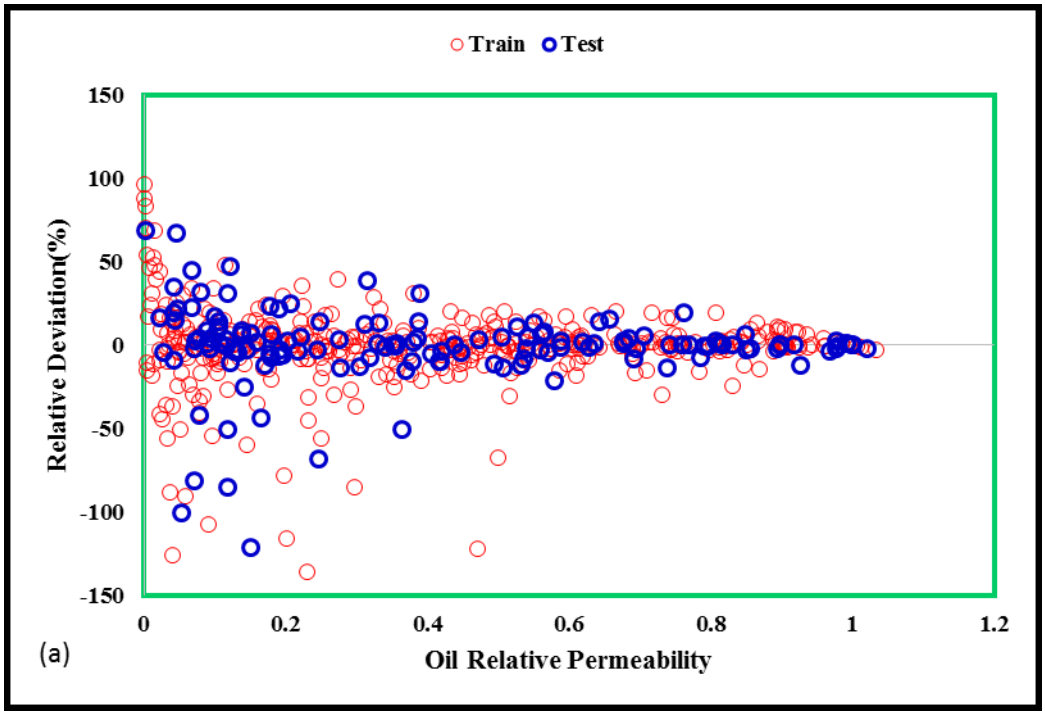

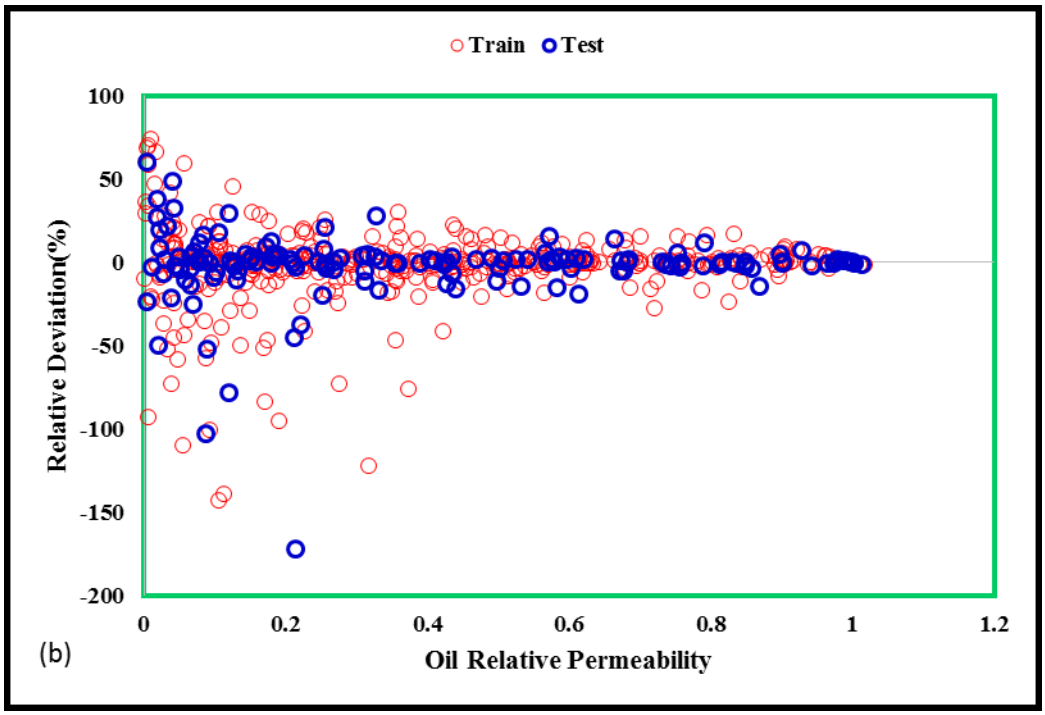

Preprints (www.preprints.org) | NOT PEER-REVIEWED | Posted: 9 July 2019 doi:10.20944/preprints201907.0129.v1

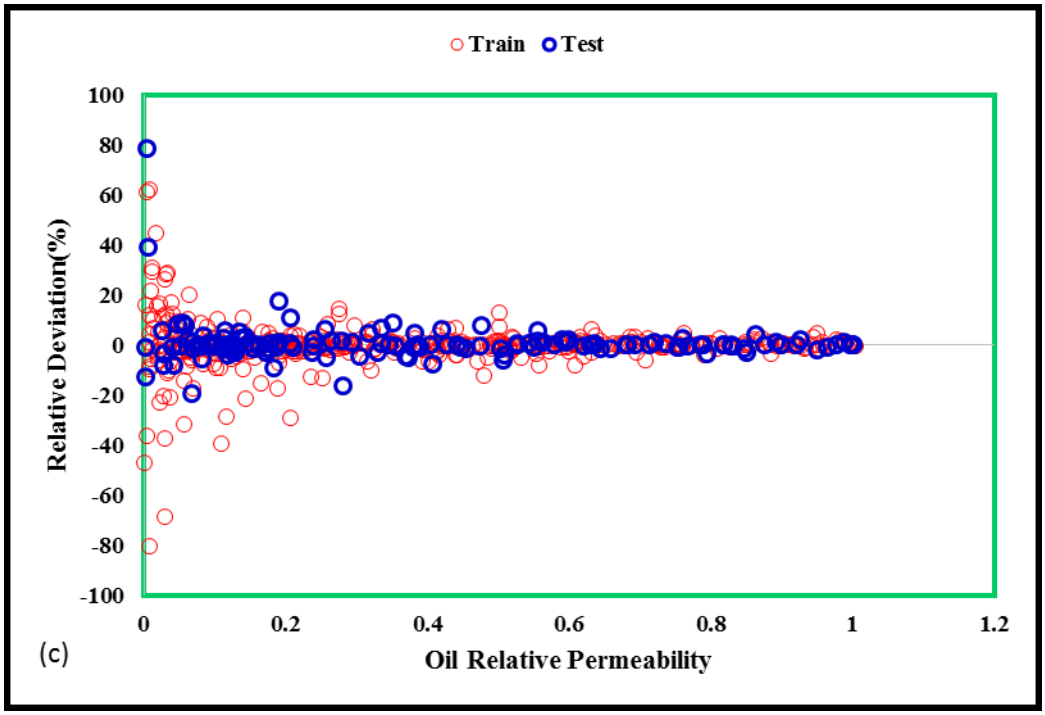

Figure 7. Relative deviation plot for: (a) ANFIS, (b) MLP-ANN, and (c) LSSVM.

Preprints (www.preprints.org) | NOT PEER-REVIEWED | Posted: 9 July 2019 doi:10.20944/preprints201907.0129.v1

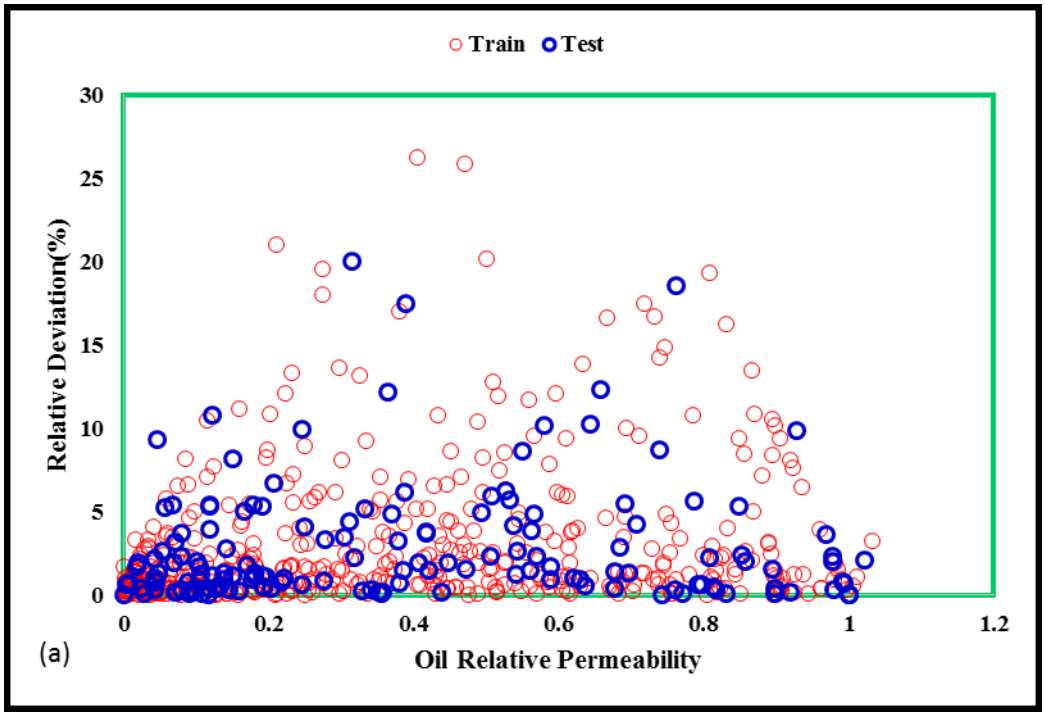

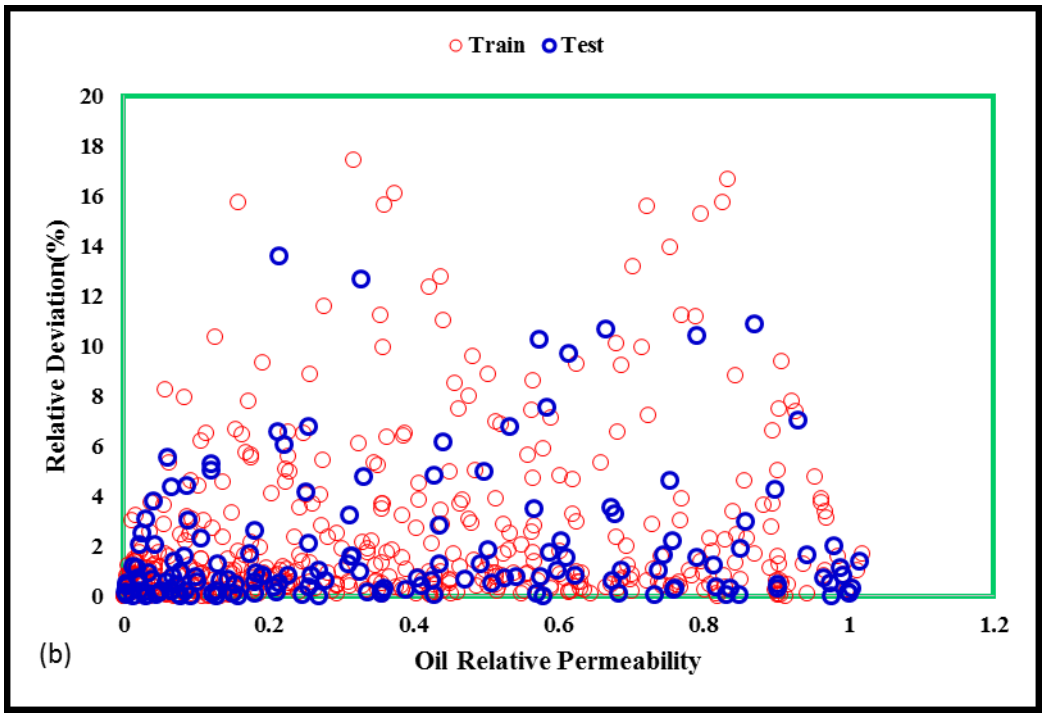

Preprints (www.preprints.org) | NOT PEER-REVIEWED | Posted: 9 July 2019 doi:10.20944/preprints201907.0129.v1

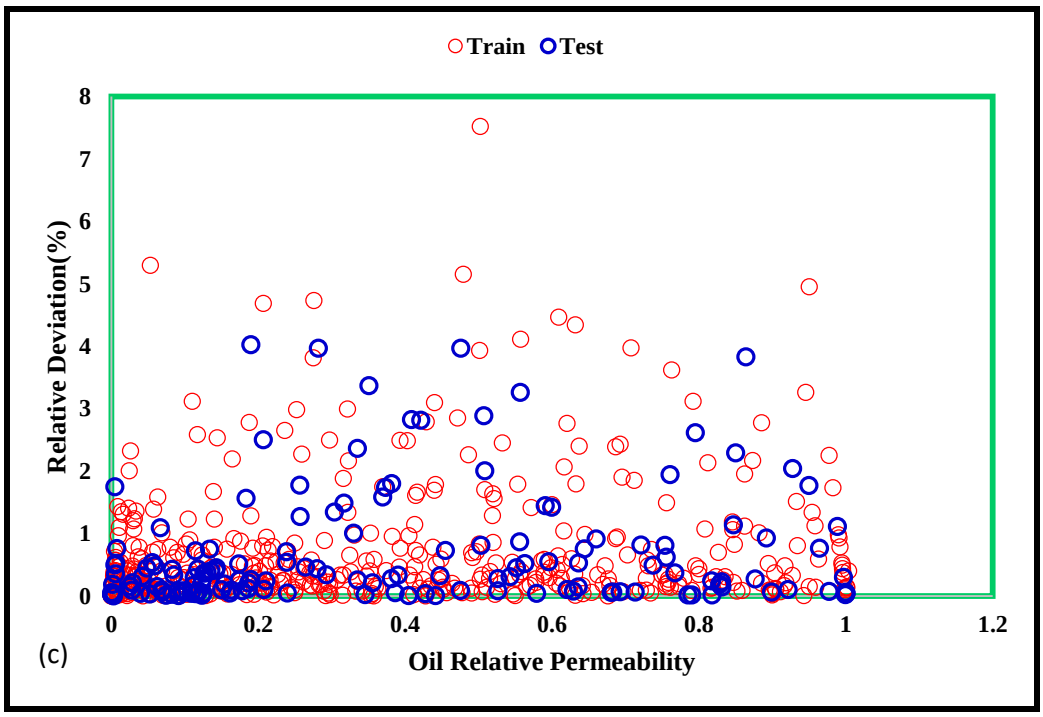

Figure 8. Absolute deviation plot for: (a) ANFIS, (b) MLP-ANN, and (c) LSSVM.

Preprints (www.preprints.org) | NOT PEER-REVIEWED | Posted: 9 July 2019 doi:10.20944/preprints201907.0129.v1

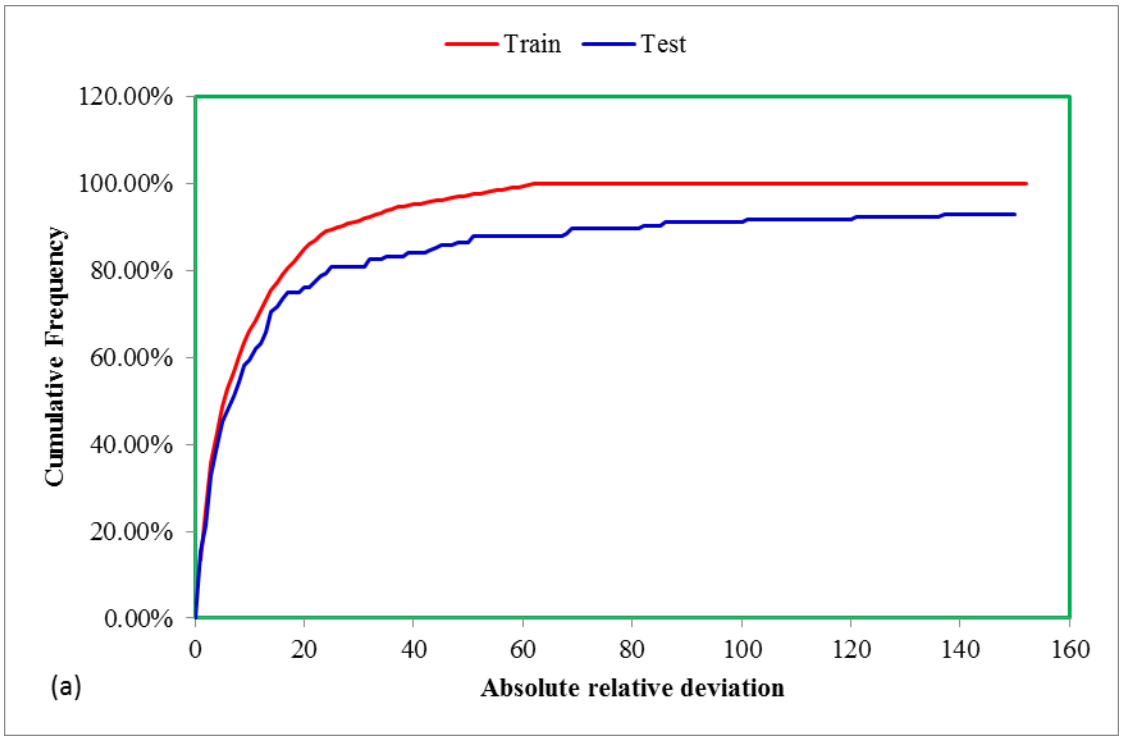

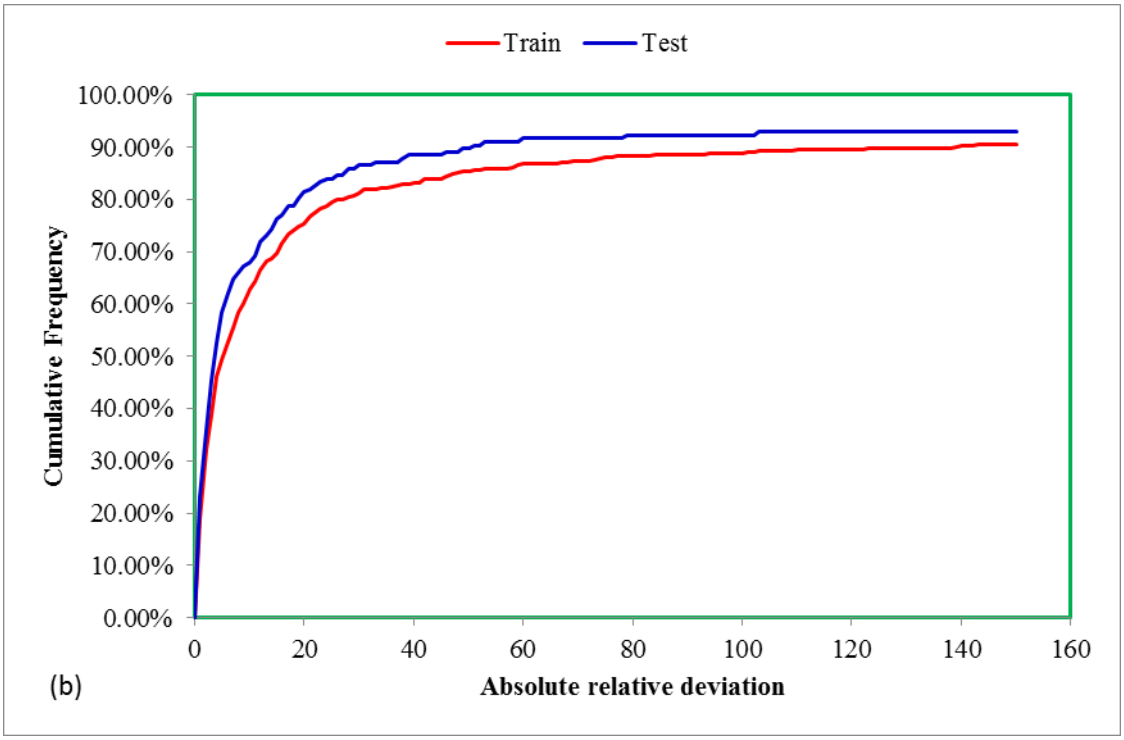

Preprints (www.preprints.org) | NOT PEER-REVIEWED | Posted: 9 July 2019 doi:10.20944/preprints201907.0129.v1

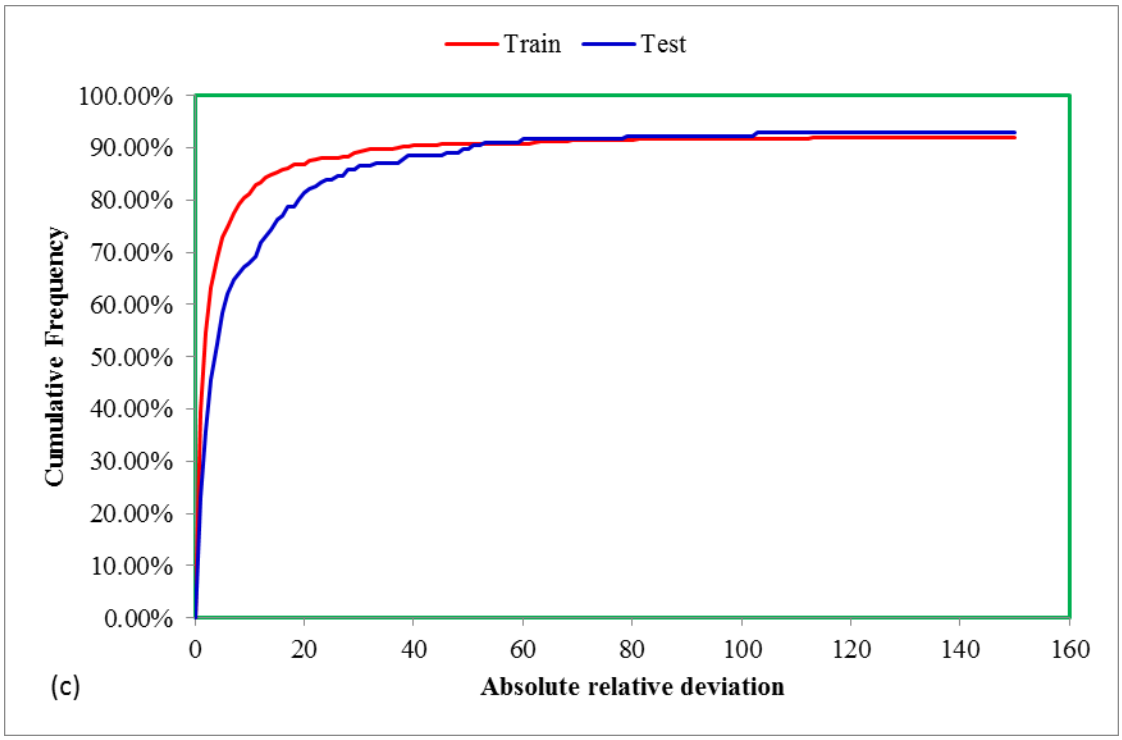

Figure 9. Cumulative frequency plot for: (a) ANFIS, (b) MLP-ANN, and (c) LSSVM.

Preprints (www.preprints.org) | NOT PEER-REVIEWED | Posted: 9 July 2019 doi:10.20944/preprints201907.0129.v1

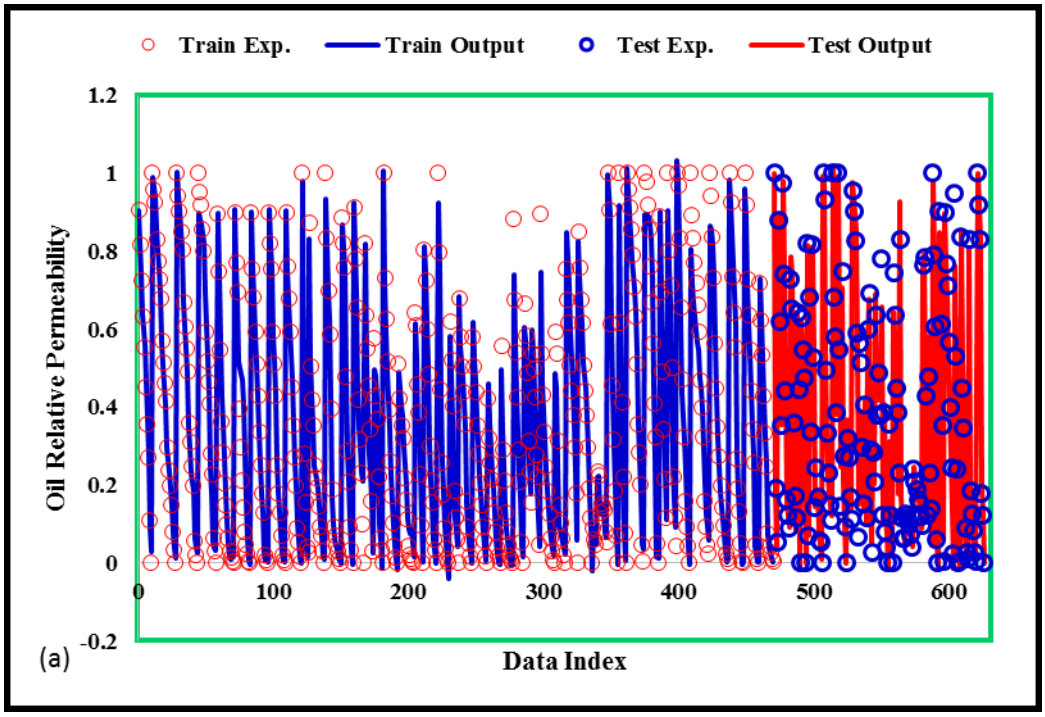

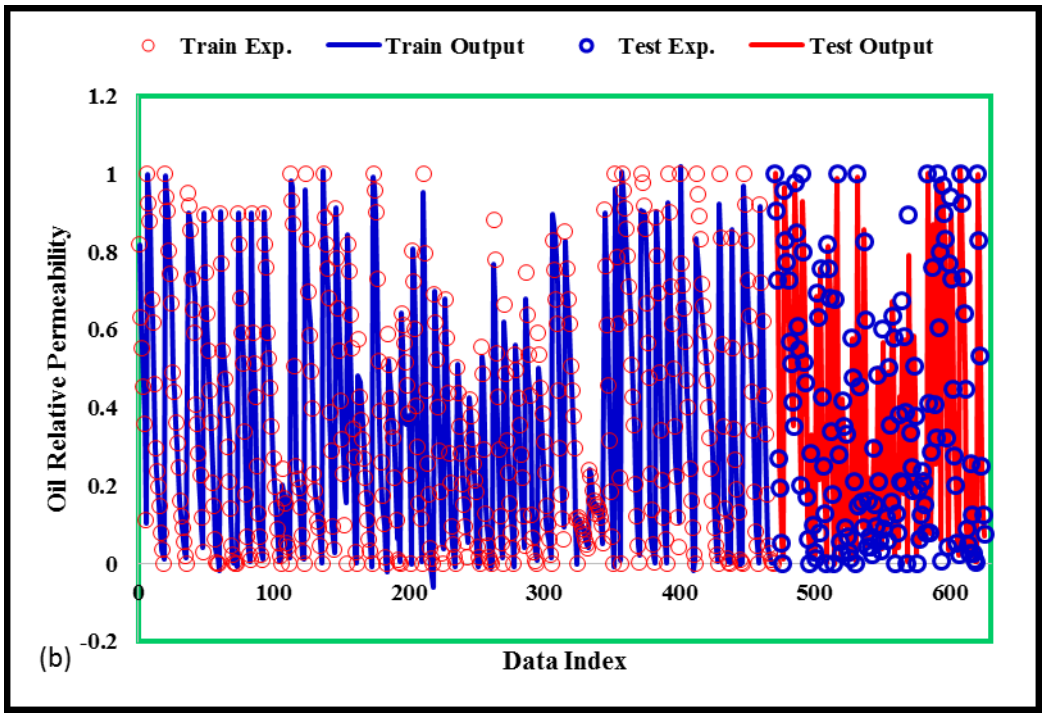

Preprints (www.preprints.org) | NOT PEER-REVIEWED | Posted: 9 July 2019 doi:10.20944/preprints201907.0129.v1

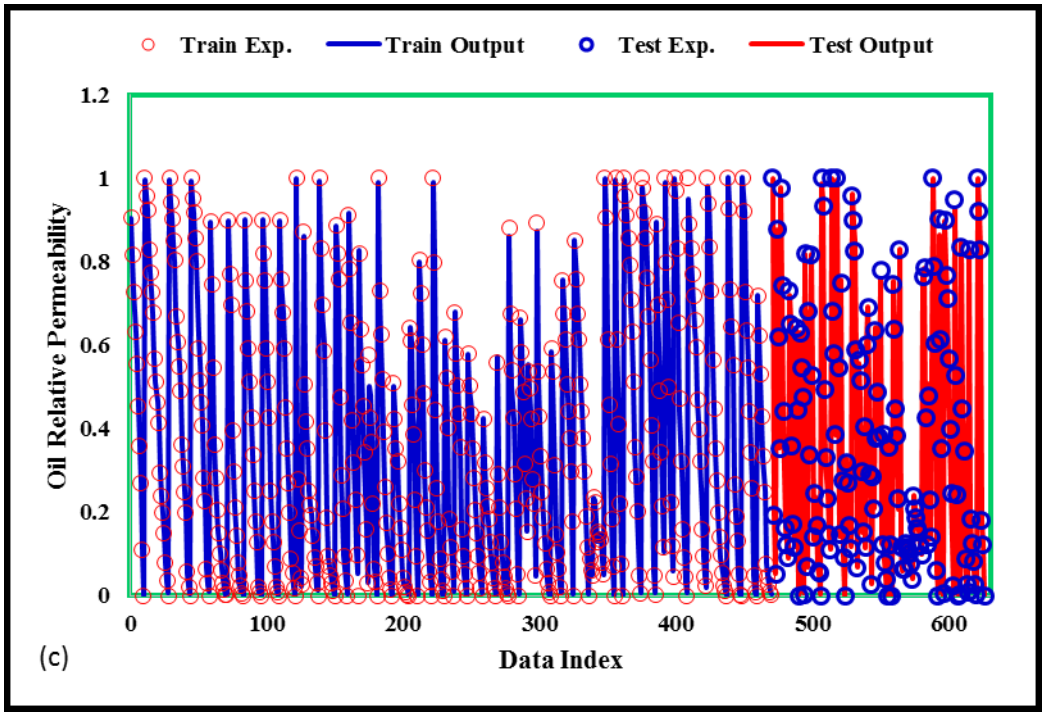

Figure 10. Simultaneous plot of the predicted and experimental values versus data points' index for: (a) ANFIS, (b) MLP-ANN, and (c) LSSVM.

Preprints (www.preprints.org) | NOT PEER-REVIEWED | Posted: 9 July 2019 doi:10.20944/preprints201907.0129.v1

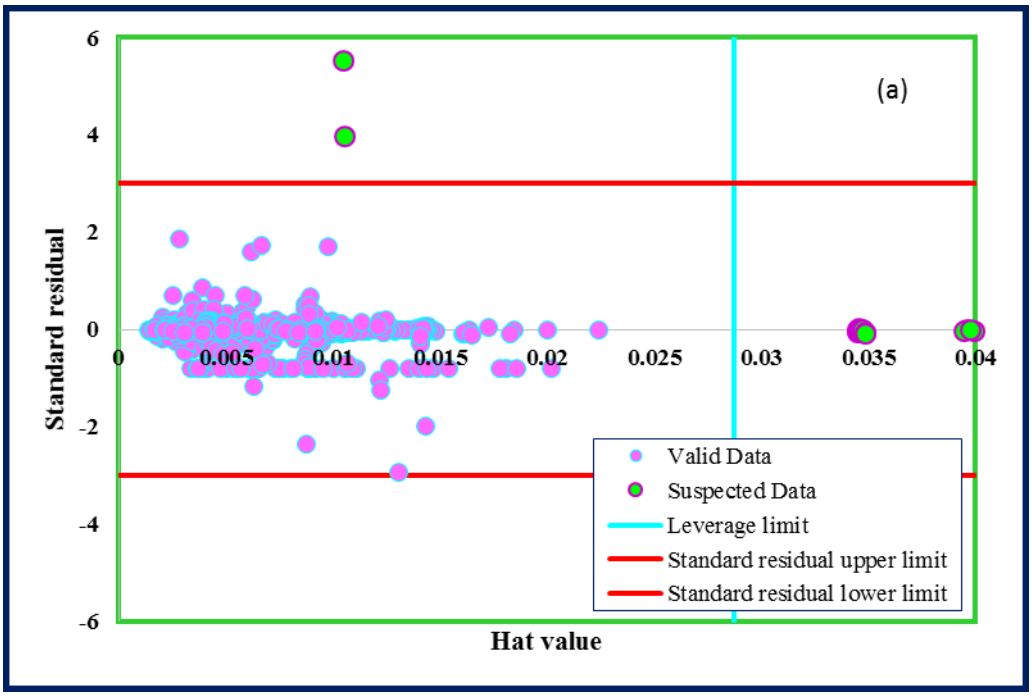

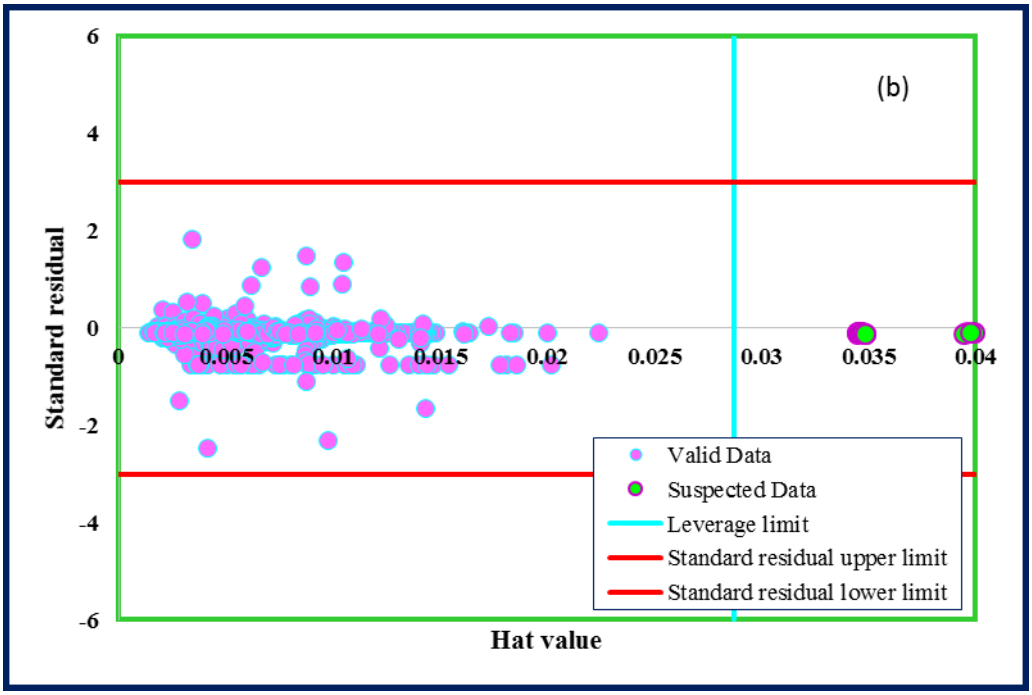

Preprints (www.preprints.org) | NOT PEER-REVIEWED | Posted: 9 July 2019 doi:10.20944/preprints201907.0129.v1

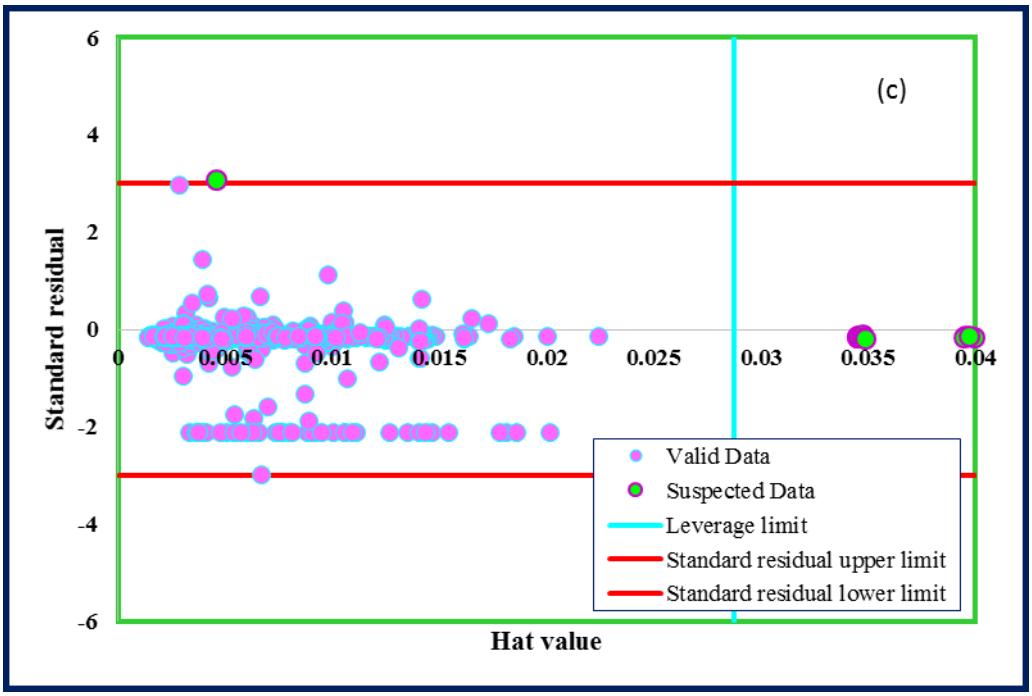

Figure 11. Williams plot of the proposed models: (a) ANFIS, (b) MLP-ANN, and (c) LSSVM.

Preprints (www.preprints.org) | NOT PEER-REVIEWED | Posted: 9 July 2019 doi:10.20944/preprints201907.0129.v1

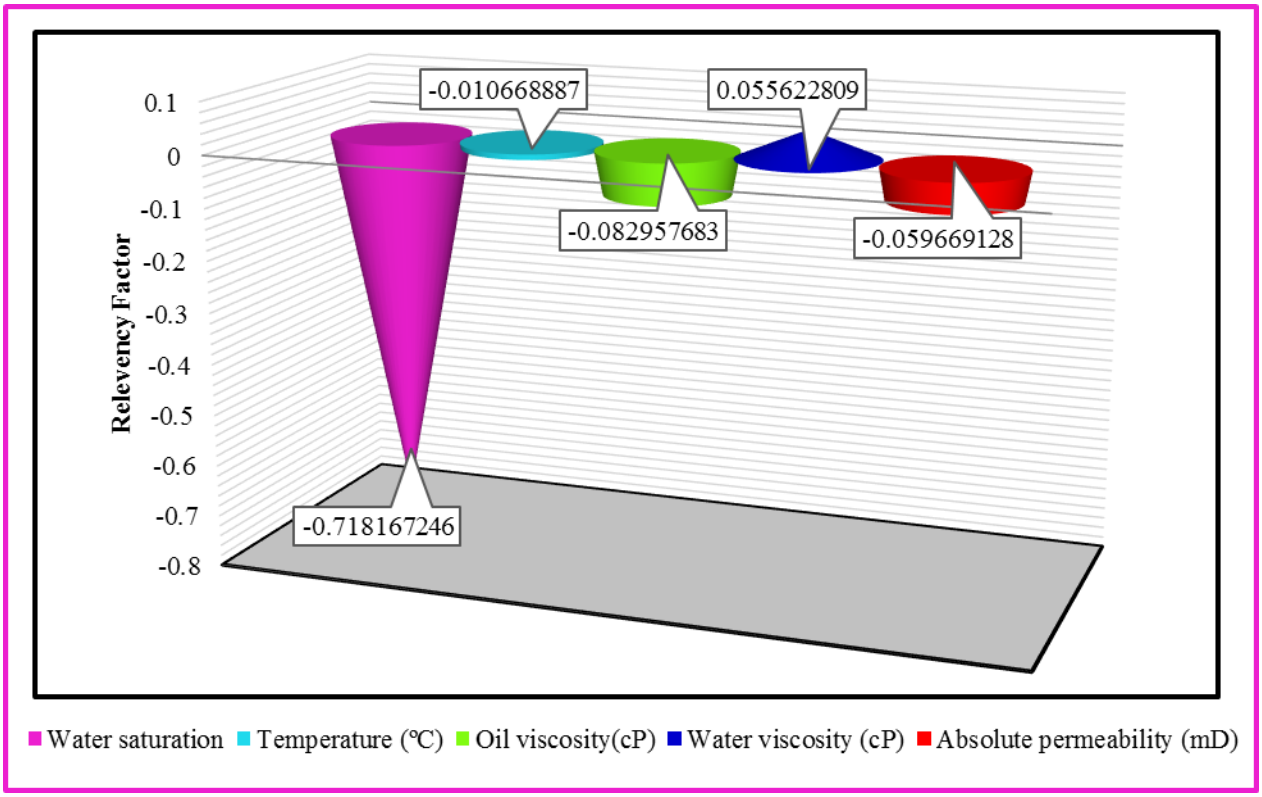

Figure 12. Sensitivity analysis results for all variables used in this study.

Preprints (www.preprints.org) | NOT PEER-REVIEWED | Posted: 9 July 2019 doi:10.20944/preprints201907.0129.v1

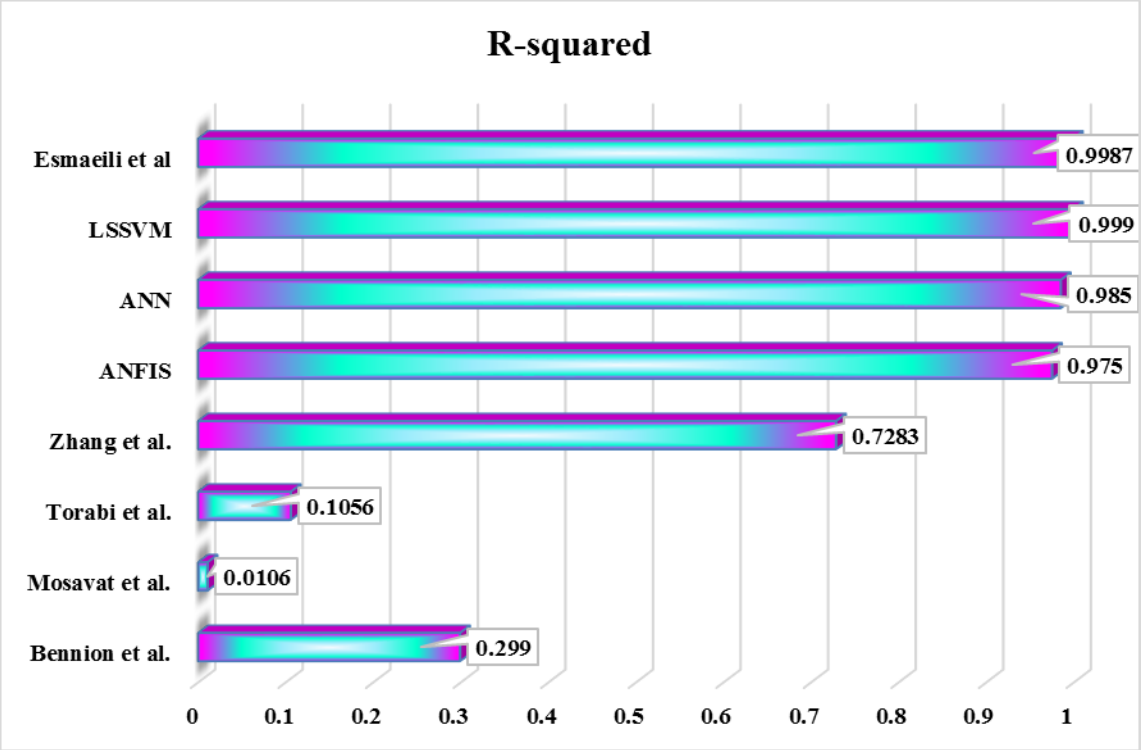

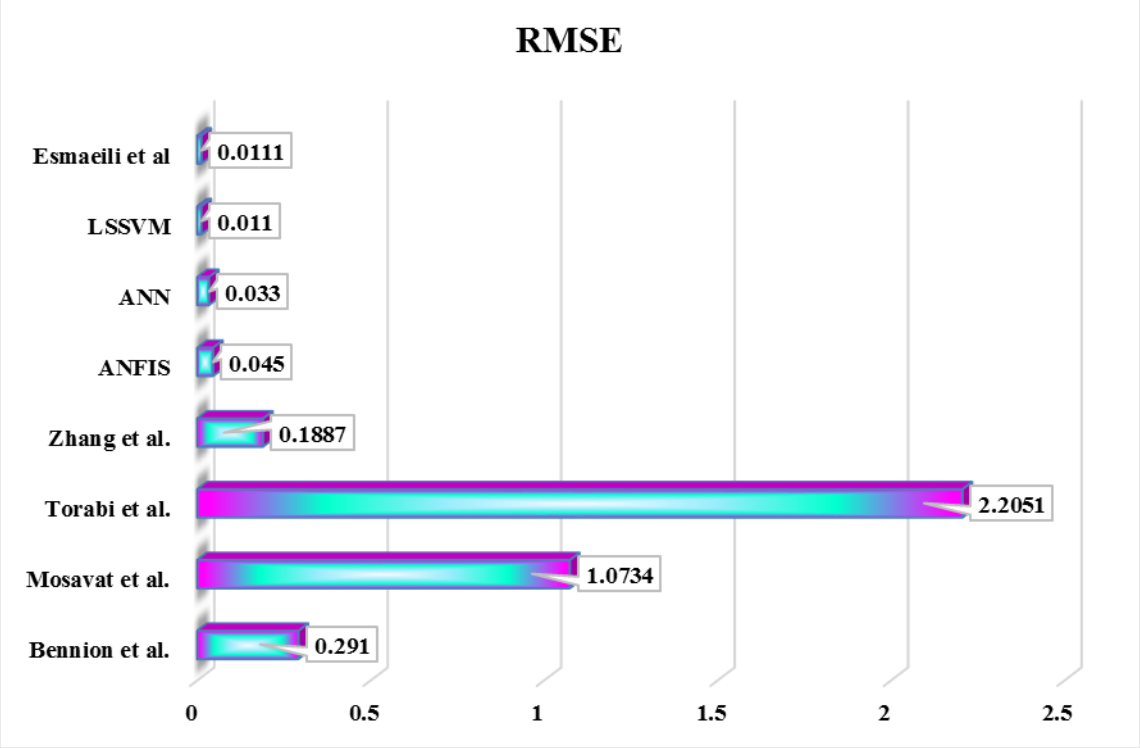

Preprints (www.preprints.org) | NOT PEER-REVIEWED | Posted: 9 July 2019 doi:10.20944/preprints201907.0129.v1

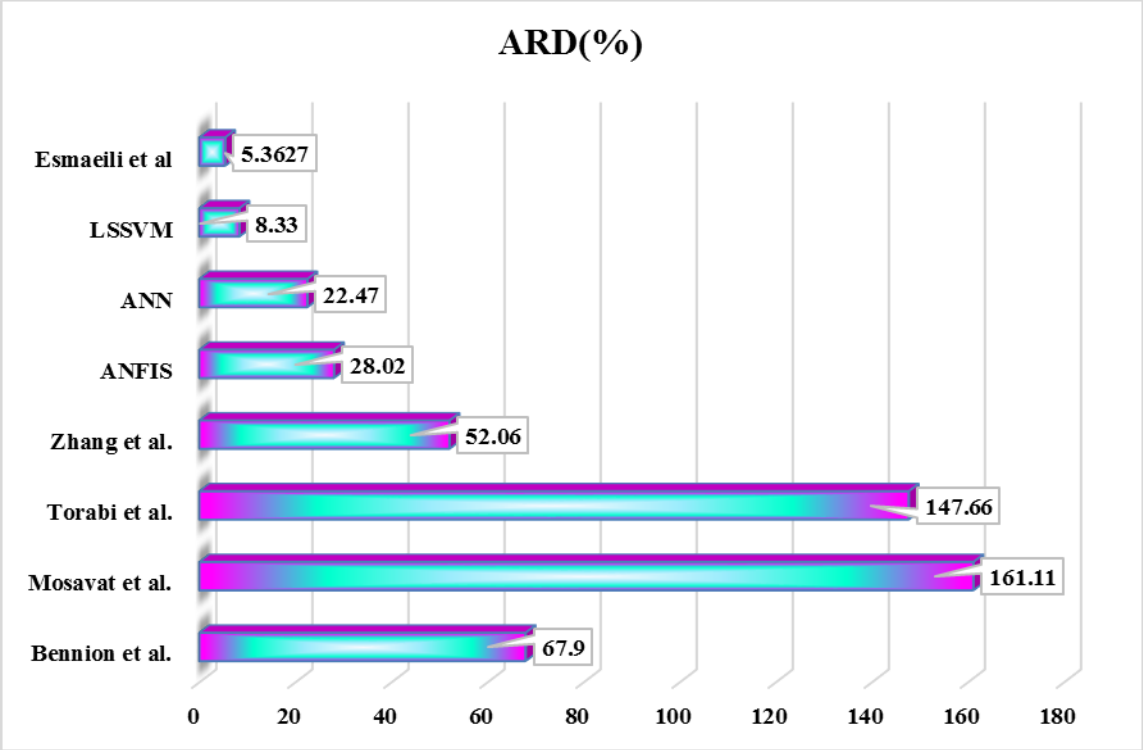

Figure 13. Comparison of previously developed models with current models

Preprints (www.preprints.org) | NOT PEER-REVIEWED | Posted: 9 July 2019 doi:10.20944/preprints201907.0129.v1

Table 2. The utilized database for development of models.

Reference	Number of data points	Temperature range (°C)	Oil viscosity range (cP)	Water viscosity range (cP)	Permeability (mD)
Ashrafi et al. [16]	169	50-140	8.3-160	0.197-0.547	42500-95000
Ashrafi et al. [15]	88	100-140	8.3-57.5	0.197-0.282	4200-95000
Lo & Mungan [20]	86	25-175	0.42-180	0.197-1.1	2770-2890
Miani & Okazawa [8]	77	22-200	2.2-1190	0.136-0.987	3093
Poston et al. [7]	75	24-135	1.9-80.2	0.212-0.914	2200-14600
Sinnokrot et al. [24]	67	21.1-162.8	2.2-173	0.147-0.946	152
Akhlaginia et al. [73]	24	28-52	220-1100	0.55-0.84	560-620
Torabi et al. [56]	24	27-45	45.5-400.2	0.623-0.852	2200-14600
Weinbrandt [17]	16	26.6-79.4	14-80	0359-0.851	851-2640

 doi:10.20944/preprints201907.0129.v1

Table 2. Details of the developed MLP-ANN model.

Type	Value/Comment
Input layer neuron	5
Hidden layer neuron	10
Hidden layer activation function	Log sigmoid
Output layer activation function	Linear
Number of data used for training	470
Number of data used for testing	156
Number of maximum iterations	1000

 doi:10.20944/preprints201907.0129.v1

Table 3. ANFIS model's detailed information.

Type	Value/Comment
Membership function	Gaussian
Maximum iterations	1000
Population size	85
Number of data used for training	470
Number of data used for testing	156
Optimization method	Particle swarm optimization
Number of clusters	10
Number of FIS parameters	120

Preprints (www.preprints.org) | NOT PEER-REVIEWED | Posted: 9 July 2019 doi:10.20944/preprints201907.0129.v1

Table 4. Statistical error analysis of the training, testing and total dataset.

Models	Error analysis			
	R^2	ARD (%)	MSE	RMSE
MLP-ANN				
Training dataset	0.983	26.878	0.002	0.040
Testing dataset	0.990	18.060	0.001	0.033
Total dataset	0.985	22.469	0.001	0.033
ANFIS				
Training dataset	0.974	30.441	0.003	0.051
Testing dataset	0.979	25.598	0.002	0.045
Total dataset	0.975	28.019	0.002	0.045
LSSVM				
Training dataset	0.999	7.730	0.000	0.012
Testing dataset	0.999	8.939	0.000	0.011
Total dataset	0.999	8.334	0.000	0.011

Preprints (www.preprints.org) | NOT PEER-REVIEWED | Posted: 9 July 2019 doi:10.20944/preprints201907.0129.v1

Table 5. Relative permeability models.

Model	k_{ro}	Experimental condition
Zhang et al. [58]	$k_{ro} = \left(\frac{1 - S_w - c_1 \ln(T) - c_2}{1 - b_1 T - b_2 - c_1 \ln(T) - c_2}\right)^{a_1 T + a_2}$ $a_1 = 0.0244 \quad a_2 = 3.8848$ $b_1 = 0.0025 \quad b_2 = 0.1941$ $c_1 = -0.1121 \quad c_2 = 0.6711$	Unsteady state Light oil Tight and stone Combination of JBN and Corey correlation 25≤T≤100 °C 4≤μ_o≤48 cP 0.153≤S_{or}≤0.324 0.234≤S_{wi}≤0.482
Torabi et al. [56]	$k_{ro} = (0.0588 P_D)^{-0.0291} \times e^{-0.01254(2-q_D)} \times (1 - S_{we})^2 \times \left(1 - S_{we}^{0.1(0.025\mu_D)^{-0.818}}\right)$ $P_D = \frac{P_{exp}}{P_{std}} \mu_D = \frac{\mu_o}{\mu_{std}} q_D = \frac{q_{exp}}{q_{std}}$	Unsteady state Heavy and light oil Berea sandstone JBN method 27≤T≤45 °C 24.3≤μ_o≤400.2 cP 0.463≤S_{or}≤0.539 0.092≤S_{wi}≤0.138
Mosavat et al. [57]	$k_{ro} = (1 - S_{we}^b)(1 - S_{we})^c$ $b = 1.02 - 0.000298(\mu_o/\mu_w) - 1.38 \times 10^{-7}(\mu_o/\mu_w)^2$ $c = 2.22 - 0.00318(\mu_o/\mu_w) - 1.22 \times 10^{-6}(\mu_o/\mu_w)^2$	Unsteady state Heavy oil Ottawa silica sand

Preprints (www.preprints.org) | NOT PEER-REVIEWED | Posted: 9 July 2019 doi:10.20944/preprints201907.0129.v1

			History match $23 \leq T \leq 100$ ℃ $19.5 \leq \mu_o \leq 1860$ cP $0.2 \leq S_{or} \leq 0.413$ $0.05 \leq S_{wi} \leq 0.105$
Bennion et al. [18]	60 ℃ < T < 100 ℃	$k_{ro} = (S_N)^{2.2}$ $S_N = (0.6 - S_w)/0.45$	Unsteady state/Steady state Heavy oil McMurray sand History match/Darcy law $10 \leq T \leq 280$ ℃ $8000 \leq \mu_o \leq 1000000$ cP $0.12 \leq S_{or} \leq 0.72$ $0.11 \leq S_{wi} \leq 0.43$
	150 ℃ < T < 275 ℃	$k_{ro} = (S_N)^3$ $S_N = (0.85 - S_w)/0.7$	